Journal of Structural Geology, Vol. 15, No. 9/10, pp. 1145 to 1168, 1993
Printed in Great Britain

0191-8141/93 $06.00+0.00

The role of dynamic recrystallization in the development of lattice preferred orientations in experimentally deformed quartz aggregates

GAYLE C. GLEASON and JAN TULLIS

Department of Geological Sciences, Brown University, Providence, RI 02912, U.S.A.

and

FLORIAN HEIDELBACH

Department of Geology and Geophysics, University of California, Berkeley, CA 94720, U.S.A.

(*Received* 16 *June* 1992; *accepted in revised form* 22 *January* 1993)

Abstract—Experiments on coaxially deformed quartz aggregates show that when dynamic recrystallization involves grain size reduction, the lattice preferred orientation (LPO) of the recrystallized grains depends on the recrystallization mechanism. At low temperatures and fast strain rates, strain-induced grain boundary migration recrystallization favors growth of grains oriented *poorly* for slip on the basal and prism planes, resulting in an LPO of *c*-axes parallel to the σ_1 direction. At higher temperatures or slower strain rates, progressive subgrain rotation produces recrystallized grains which inherit the small-circle girdle LPO of their deformed host grains and which continue to re-orient by slip. At even higher temperatures and slower strain rates, progressive subgrain rotation is accompanied by rapid grain boundary migration, which does not favor grains of any particular orientation; thus the LPO is again similar to that of non-recrystallized grains. In contrast, when dynamic recrystallization involves grain growth driven by surface energy reduction, a strong LPO of *c*-axes parallel to σ_1 develops during grain growth but then evolves with increasing strain toward a small-circle girdle. The correlation of LPOs with recrystallization mechanisms has important implications for the assumption of homogeneous strain in theoretical models of LPOs and for interpreting natural LPOs in recrystallized rocks.

INTRODUCTION

LATTICE preferred orientations (LPOs) have been recognized in a wide variety of tectonites from the crust and upper mantle. Combined with other observations, they can be used to determine the relative contributions of coaxial and non-coaxial strain (e.g. Schmid & Casey 1986) and the sense of shear (e.g. Simpson & Schmid 1983). In addition, they may contain information on the temperature and strain rate of deformation; however, the ability to make such interpretations depends on a detailed understanding of the orienting processes involved.

Most of the analyses of quartz LPOs have assumed that they result from external rotations accompanying intracrystalline slip. The patterns produced depend on the active slip systems and their relative critical resolved shear stresses, which in turn depend on temperature, strain rate and 'water' content. The dominant slip systems in quartz are reasonably well known (e.g. Hobbs 1985), and have been used in computer models to predict the LPOs resulting from different strain geometries. Early Taylor–Bishop–Hill (TBH) models assumed perfect plasticity and homogeneous strain, requiring five independent slip systems (e.g. Lister *et al.* 1978, Lister & Hobbs 1980). More recently, Wenk *et al.* (1989) developed a visco-plastic, self-consistent model, allowing heterogeneous strain as well as strain rate dependence. This model has successfully reproduced many of the main features of LPO patterns for non-recrystallized quartz aggregates, but does not predict the strong *c*-axis maximum in the intermediate strain direction which is common in natural tectonites.

Many quartz-rich tectonites are dynamically recrystallized, and there has been some discussion as to whether the processes controlling the LPOs of these rocks are the same as those in non-recrystallized rocks. Lister & Price (1978) suggest that since slip remains the strain-producing mechanism in recrystallized aggregates, the LPOs of such aggregates should be successfully predicted by slip models, such as those described above. Others have suggested that strain-induced grain boundary migration allows some orientations to grow at the expense of others, resulting in LPOs different than those produced by slip (e.g. Green *et al.* 1970, p. 320). Recently Jessell (1988a,b) and Jessell & Lister (1990) have modified the TBH model to incorporate grain boundary migration in addition to slip. However, the orientations they assumed to be favored by grain boundary migration were based on observations of experimentally deformed ice, camphor and octochloropropane, and may not be appropriate for quartz.

Early experimental studies on the effects of dynamic recrystallization on the LPO of olivine produced conflicting results. Ave'Lallemant (1975) and Kunze & Ave'Lallemant (1981) found that the LPOs of grains recrystallized during simple shear differed from those of non-recrystallized grains, whereas Toriumi & Karato (1985) found that the LPOs of dynamically recrystallized olivine grains were similar to those of the non-

recrystallized grains. Recent work by Karato (1987, 1988) helped to resolve this conflict by demonstrating that the mechanism of dynamic recrystallization of olivine varies with temperature and strain rate and that the LPO depends on the mechanism of recrystallization.

An assessment of the effect of dynamic recrystallization on the LPOs of quartz aggregates depends on accurate identification of the recrystallization mechanisms. Recently, three regimes of dislocation creep, involving different mechanisms of dynamic recrystallization, have been identified for quartz aggregates (Hirth & Tullis 1992). With increasing temperature, increasing water content or decreasing strain rate, and thus decreasing flow stress, these recrystallization mechanisms are as follows: (1) strain-induced grain boundary migration recrystallization (Sellars 1978, Tullis & Yund 1985, Hirth & Tullis 1992); (2) progressive subgrain rotation recrystallization (White 1976, Guillope & Poirier 1979, Hirth & Tullis 1992); and (3) progressive subgrain rotation with rapid grain boundary migration (Guillope & Poirier 1979, Hirth & Tullis 1992). It is important to realize that these regimes depend on the relative rates of dislocation production, dislocation climb and grain boundary migration which in turn are controlled by the deformation parameters. A more complete discussion of how changes in these parameters control which mechanism is dominant can be found in Hirth & Tullis (1992, pp. 154–155).

In this paper we present the results of an experimental study of quartz LPOs resulting from dynamic recrystallization by each of these three mechanisms. For aggregates in which recrystallization involves a grain size reduction, we compare the LPOs of deformed original grains with those of dynamically recrystallized grains in each dislocation creep regime. In addition, we present results for deformed fine-grained aggregates in which dynamic recrystallization involves grain growth. Our results show that the LPOs of recrystallized grains deviate substantially from those produced by slip if the rate of grain boundary migration is fast compared to the rate of deformation as predicted by Karato (1987); this occurs in the lowest temperature dislocation creep regime, or in extremely fine-grained and 'wet' aggregates. In these cases, strain is inhomogeneous and models assuming homogeneous strain will not predict the correct LPO.

METHODS

This study combines new data on preferred orientations and observations of microstructures with data previously reported (Tullis 1971, Tullis *et al.* 1973, Hirth & Tullis 1992). The experimental conditions for all samples included in this study are listed in Table 1. Samples deformed prior to this study are listed with their appropriate reference. The microstructures of some of the samples from previous studies were analyzed in TEM for this study in order to verify the mechanism of recrystallization and thus the dislocation creep regime. The LPOs of the samples from Tullis (1971) and Tullis *et al.* (1973) were measured and analyzed during those earlier studies by the X-ray goniometric methods described by Baker *et al.* (1969), whereas the LPOs for the other samples were measured specifically for this study by the methods described below.

Starting materials

The four quartz aggregates used in this study have <1% impurities, and no initial shape or lattice preferred orientation. All aggregates contain about 0.2 wt % water, except for the Dover flint which contains up to 2 wt %. All of these aggregates have been used in previous experimental studies, and more detailed descriptions can be found in the references listed. The Quadrant quartzite has an average grain size of 150 μm (Ave'Lallemant & Carter 1971, Tullis *et al.* 1973). The Black Hills quartzite has an average grain size of 100 μm (Tullis *et al.* 1973, Mainprice & Paterson 1984, Dell'Angelo & Tullis 1989, Hirth & Tullis 1992). One novaculite has an average grain size of 4 μm (Kronenberg & Tullis 1984), and the other novaculite has an average grain size of 2 μm (Hirth & Tullis 1992). Dover flint has an average grain size of 1 μm (Green *et al.* 1970, Tullis & Yund 1982, Mainprice & Paterson in press).

Experimental procedures

Cylindrical samples (0.63 cm diameter, 1.3 cm length) were jacketed in either Ag or Pt (0.25 mm thick) and mechanically sealed with Pt end discs, although in a few cases when talc was used as the confining medium, no jacket was used. Most samples were bench-dried ('as-is'), although a few had 0.17 wt % water added.

Samples were deformed in axial compression in a modified Griggs-type apparatus, using NaCl, KCl, AlSiMag, soft-fired pyrophyllite or talc as the confining media. The deformation conditions spanned the three dislocation creep regimes identified by Hirth & Tullis (1992), and included pressures from 1.0 to 1.25 GPa, temperatures of 700–1200°C and constant displacement rates of $1.9 \times 10{-}5$, $1.9 \times 10{-}6$ or $1.9 \times 10{-}7$ cm s-1, corresponding to strain rates of $1.5 \times 10{-}5$, $1.5 \times 10{-}6$ and $1.5 \times 10{-}7$ s-1, respectively. Samples were shortened by varying amounts (up to 75%) in order to document the evolution of the LPOs with increasing strain. The final shape of each sample was axisymmetric.

Deformed samples were impregnated with epoxy and one to three longitudinal sections were made, for petrographic and transmission electron microscope (TEM) observations (using a Phillips EM420 TEM at 120 kV), and for X-ray pole figure goniometer measurements.

LPO measurement techniques

In partially recrystallized samples, the *c*-axis LPOs of non-recrystallized grains were measured on a universal stage. Measurements of 300–500 contiguous grains were

Table 1. Experimental conditions for all samples included in study

Sample No.	E (log 10 s^{-1})	Temp. (°C)	P_{con}* (MPa ± 5%)	$\sigma_1 - \sigma_3$† (MPa)	% ε‡	Confining medium	Starting material	Water content (wt%)	Reference
Regime 1:									
GB-219	−6	700	1250	2390	27/49	talc	QQ		Tullis (1971)
GB-309	−6	700	1290	2350	34/60	talc	QQ		Tullis (1971)
GB-177	−6	700	1290	2400	45/75	talc	QQ		Tullis *et al.* (1973)
W-340	−6	700	1180	900	20	NaCl	HQ		Hirth & Tullis (1992)
CQ-83	−5	750	1140	550	45	NaCl	DN	0.17	Hirth & Tullis (1992)
Regime 2:									
CQ-73	−6	800	1100	290	30	NaCl	BHQ		Hirth & Tullis (1992)
CQ-94	−6	700	1140	350	55	KCl	DN	0.17	Hirth & Tullis (1992)
BA-20	−6	800	1020	700	50/57	talc	BHQ		
GB-332	−6	900	1000	1630	51/65	AlSiMag	QQ		Tullis (1971)
GB-438	−6	900	1000	1580	45/70	AlSiMag	BHQ		Tullis (1971)
GB-444	−6	900	930	2180	75/90	AlSiMag	BHQ		Tullis (1971)
BA-14	−6	900	1180	200	52	NaCl	BHQ		
NV-53	−6	850	1160	250	58	NaCl	novaculite	0.03	Kronenberg & Tullis (1984)
BA-9	−5	1100	900	300	51	pyroph	BHQ		
Regime 3:									
CQ-78	−6	900	1140	150	37	NaCl	BHQ	0.16	Hirth & Tullis (1992)
BA-42	−6	900	1140	200	50	NaCl	BHQ	0.16	
W-426	−5	1200	1040	400	60	AlSiMag	BHQ		
GB-426	−7	1000	930	1500	52/76	AlSiMag	BHQ		Tullis (1971)
Grain growth:									
BA-34	−5	800	1140	200	30	NaCl	DF		
BA-22	−5	800	1250	320	70	NaCl	DF		
BA-27	−5	900	1220	100	14	NaCl	DF		
BA-30	−5	900	1140	170	20	NaCl	DF		
BA-26	−5	900	1250	260	30	NaCl	DF		
CQ-76	−5	900	990	150	48	NaCl	DF		
BA-51	−5	900	1180	220	52	NaCl	DF		
BA-21	−5	900	1230	350	60	NaCl	DF		
BA-25	−5	900	1250	200	75	NaCl	DF		
BA-29	−6	800	1100	150	30	NaCl	DF		
CQ-84	−6	900	1140	250	57	NaCl	DN	0.17	Hirth & Tullis (1992)

*These confining pressure values are 76% of the nominal confining pressure measured during the experiment. We have determined, using the wollastonite–garnet structure transition of $CaGeO_3$, that the nominal pressure is systematically over estimated by 24% in a standard experimental assembly with NaCl as the confining medium. Talc, pyrophyllite and AlSiMag as confining media may result in even larger over estimates.

†The strength of the confining media and friction in the talc, AlSiMag and pyrophyllite assemblies result in anomalously high differential stresses.

‡Strain = [(initial length − final length)/initial length] × 100. Two values for strain indicate sample deformation was heterogeneous. First value is total sample strain and second value is local strain in region of highest strain.

made in the most homogeneously deformed central part of each sample. For grains with undulatory extinction, the orientation of the center of the grain was taken as the 'average'. Because the deformation geometry of each sample was axi-symmetric, a *c*-axis profile could be constructed by plotting the data on equal-area Schmidt stereographic nets, counting the numbers of grains within small-circle girdles at 5° increments, and converting the numbers to concentrations by dividing the fractional number of grains in each annulus by the fractional area of the hemisphere in each annulus. The concentrations were then plotted on a histogram to form a profile. These profiles were compared to *c*-axis profiles derived from X-ray data. The *c*-axis LPO patterns determined from X-ray goniometer methods tend to be more diffuse than those determined from universal stage measurements, because the X-ray LPOs reflect the true volume average of the sample, and hence include the subgrains and any recrystallized grains away from the centers of the non-recrystallized grains.

The bulk LPOs of a number of highly recrystallized samples were measured by X-ray diffraction (CuK_α radiation, $\lambda = 1.54$ Å) on a Norelco pole figure goniometer in transmission geometry (e.g. Baker *et al.* 1969). Sections of 100 μm thickness were prepared parallel to the compression direction. Previous studies by Baker *et al.* (1969) demonstrated that axi-symmetric compression experiments result in axi-symmetric LPOs, thus we assumed radial symmetry of the preferred orientation around the compression direction. Therefore, we did not measure complete pole figures, but scanned from parallel to the compression direction (angle $\phi = 0$) a total of 360° in steps of 2.5° within a single plane containing σ_1. The measured area (spot size of the X-ray beam) on the sample was a circle of about 1 mm diameter. The variation in orientation of six lattice planes ($\{10\bar{1}0\}$, $\{11\bar{2}0\}$, $\{10\bar{1}1\}+\{01\bar{1}1\}$, $\{20\bar{2}1\}$ + $\{02\bar{2}1\}$, $\{10\bar{1}2\}+\{01\bar{1}2\}$, $\{11\bar{2}2\}$) was recorded.

The scans for each sample were corrected for incoherent background, normalized and then converted into axially symmetric pole figures which served as data for the calculation of the complete orientation distribution function (ODF) with the WIMV algorithm (abbreviated after its authors Williams, Imhof, Matthies and Vinel;

for a detailed description see Matthies 1979, Kallend *et al.* 1991). The WIMV method uses an iterative approach to calculate the ODF from the experimental pole figures. The quality of the ODF is estimated by comparing experimental and recalculated pole figures and is expressed in a 'reproduction' or 'RP' value (Matthies *et al.* 1988). The 'RP' value gives the deviation between calculated and measured intensities averaged over each scan and all measured lattice planes (*hkl*s) for one sample. In our calculation 'RP' values ranged from 0.4 to 2.9%, which we consider satisfactory.

The calculation of the ODF in this study was useful for three reasons. First, comparison of measured and recalculated pole figures provides valuable information about the compatibility of the different scans for each sample, i.e. the consistency of our measurements. Second, the *c*-axis distribution, which cannot be measured directly with X-rays, can be calculated from the ODF (as can the pole figure of any other *hkl*), so that the results are easy to compare with those from universal stage measurements. Thirdly, the ODF allows us to derive an inverse pole figure, i.e. the distribution of a sample co-ordinate such as the compression axis with respect to the crystal co-ordinates. In addition the WIMV algorithm also allows for a differentiation between positive and negative forms, for example $\{10\bar{1}1\}$ and $\{01\bar{1}1\}$, by distinguishing their different contributions in intensity to the measured profile.

Eight samples were measured with X-ray diffraction and processed with the WIMV algorithm. The results of the calculations are demonstrated in detail for two characteristic types of preferred orientation found in this study. Sample CQ-76 (flint, 100% recrystallized) shows a strong concentration of quartz *c*-axes parallel to the compression direction, while sample BA-42 (quartzite, ~90% recrystallized) exhibits a small-circle distribution of *c*-axes around the compression direction. Figure 1 displays the measured and recalculated intensity profiles for all six diffraction peaks of both samples. The calculated intensity distributions contain all significant features of the experimental scans and reflect the measured preferred orientations with great accuracy. Generally, they are slightly smoother than the experimental intensity distributions.

In Fig. 2, the contributions of positive and negative forms to the scans of $\{10\bar{1}1\}+\{01\bar{1}1\}$, $\{10\bar{1}2\}+\{01\bar{1}2\}$ and $\{20\bar{2}1\}+\{02\bar{2}1\}$ are plotted separately for both samples. While the intensity distributions of the two forms are nearly identical for CQ-76, they are significantly different for sample BA-42. This difference also is reflected in the symmetry of the inverse pole figures of the two samples (Figs. 11a and 13b). The inverse pole figure of CQ-76 (Fig. 13b) is centrosymmetric around (0001) whereas the intensities for the positive forms are significantly higher (Fig. 11a) in sample BA-42 (compare with scans on Figs. 1 and 2 at $\phi = 0°$). The asymmetry in the inverse pole figures of most samples can be explained by the operation of mechanical Dauphine twinning (Tullis & Tullis 1972, Tullis *et al.* 1973), in which stress applied normal to negative forms will cause them to switch to the equivalant positive form (e.g. $\{01\bar{1}1\}$ to $\{10\bar{1}1\}$). Because the Dauphine twin plane contains the *c*-axis, samples with a *c*-axis maximum parallel to the compression axis (e.g. CQ-76) will not undergo Dauphine twinning and thus will have symmetric inverse pole figures. However, samples in which the *c*-axes form small-circle girdles about the compression axis (e.g. BA-42) will undergo twinning and thus exhibit asymmetric inverse pole figures.

RESULTS I: RECRYSTALLIZATION RESULTING IN GRAIN SIZE REDUCTION

In this section we first document the LPOs of dynamically recrystallized grains developed by grain size reduction in each of the three dislocation creep regimes identified by Hirth & Tullis (1992), in order of increasing temperature. For each regime, we first briefly summarize the deformation and recovery mechanisms and characteristic microstructures. Then we illustrate the *c*-axis LPOs of non-recrystallized grains, as well as those of dynamically recrystallized grains. The experimental conditions corresponding to each regime can be found in fig. 1 in Hirth & Tullis (1992). The transitions between regimes are gradual; in most cases, deformation conditions were chosen to be well within the regimes in order to evaluate the effects of the dominant recrystallization mechanism. A list of experiments is given in Table 1.

Regime 1: *strain-induced grain boundary migration*

Dislocation creep in regime 1 occurs at relatively low temperatures, fast strain rates and high differential stress, where dislocation climb is too slow to offset work hardening (Tullis & Yund 1985, Hirth & Tullis 1992). The difficulty of climb is indicated at the TEM scale by high dislocation densities, dislocation tangles, a cell structure and many straight dislocation segments. These structures produce the patchy extinction, deformation bands and lamellae seen at the optical scale (Fig. 3a). Original grains are inhomogeneously deformed and are gradually replaced by recrystallized grains. The small, dislocation-free recrystallized grains are produced by grain boundary bulging, driven by local differences in dislocation densities; at the TEM scale, grain boundaries are convex towards regions of high dislocation densities (Fig. 3b). Grain boundary migration recrystallization acts as a recovery mechanism because the strain-free, recrystallized grains can undergo an increment of 'easy' glide before becoming work hardened and replaced by a new episode of grain boundary migration. At any given time, some recrystallized grains will have a high density of dislocations and others will have none. Because the recrystallized grains are weaker than the original grains, sample strength varies with the amount of recrystallization. Initially, the sample undergoes work hardening until an interconnected network of recrystallized grains develops. Then, strain weakening

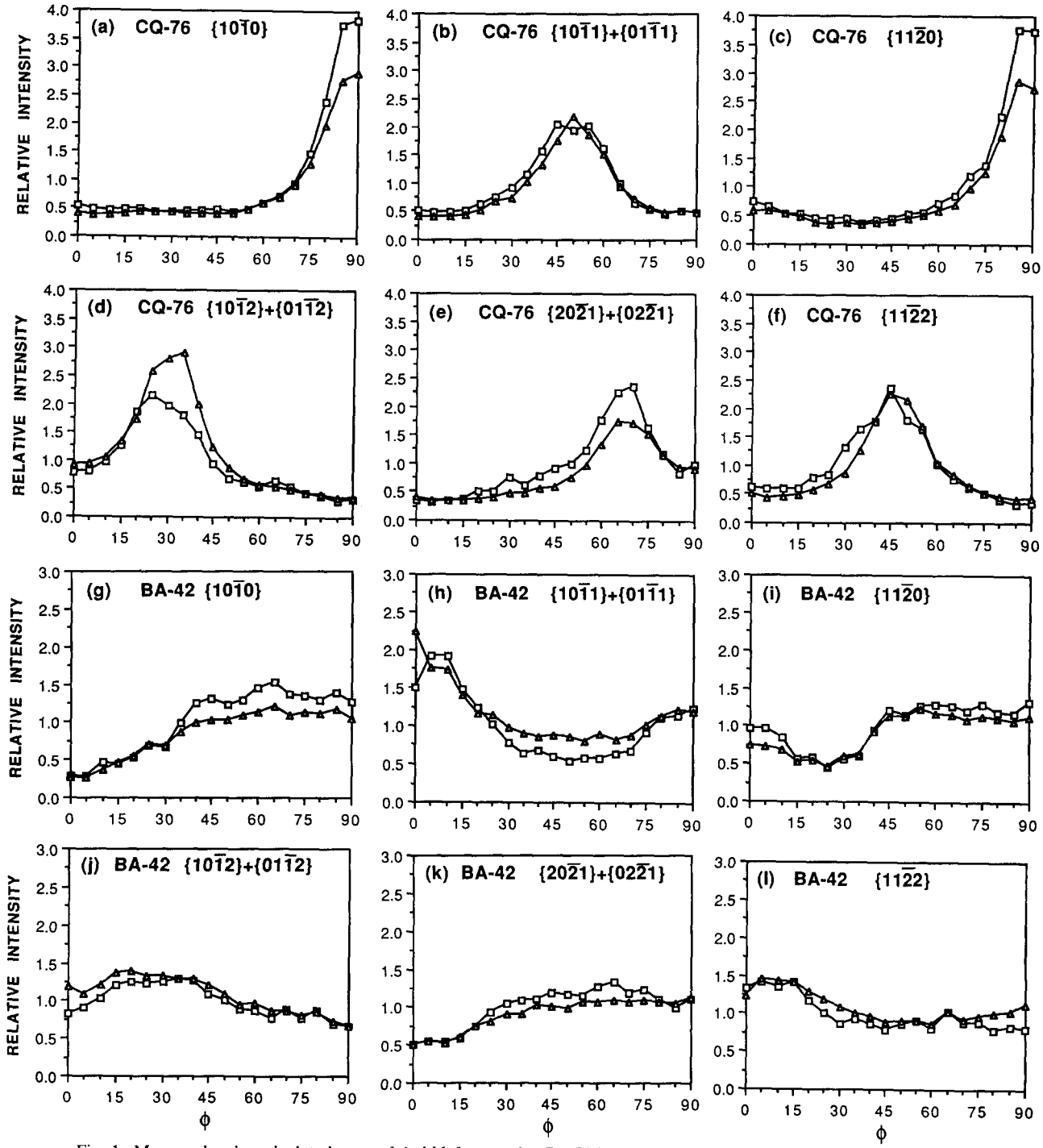

Fig. 1. Measured and recalculated scans of six *hkl*s for samples CQ-76 (a–f) and BA-42 (g–l). Squares are measured scans, triangles are recalculated scans. ϕ is the angle between σ_1 and the poles to the planes of the forms indicated. Relative intensity is in multiples of uniform distribution.

accompanies progressive recrystallization until steady state strength, grain size and microstructure are reached at ~100% recrystallization (Tullis & Yund 1985, Hirth & Tullis 1992).

Non-recrystallized grains. The *c*-axis LPOs of non-recrystallized grains deformed in regime 1 were determined previously for three quartzite samples shortened 49, 60 and 75%, respectively (Tullis 1971). In all of the samples, the non-recrystallized grains have patchy extinction, deformation bands and deformation lamellae (Fig. 3a). Although the average aspect ratio of the non-recrystallized grains increases with increasing strain, the deformation is quite heterogeneous, and some equant grains remain in the most highly strained sample.

Profiles showing the density of *c*-axes as a function of angle (ϕ) to the maximum compressive stress direction (σ_1) were constructed for all three samples from LPO data obtained previously by X-ray pole figure goniometer methods (Tullis 1971) and calculated from inverse pole figures by the method described in Baker *et al.* (1969). The *c*-axis profile for the intermediate strain sample (GB-309) is shown in Fig. 7(a); it shows a maximum of *c*-axes at ~20° to σ_1 (equivalent to a

small-circle girdle about σ_1 with an opening angle of 20°), with a greater than uniform concentration parallel to σ_1. The strength of the preferred orientation increases with increasing strain. Only ~2% of the lowest strain (49%) sample is recrystallized, and only ~7% of the intermediate strain (60%) sample is recrystallized. Thus we infer that this pattern has not been affected by recrystallization and is due to intracrystalline slip, primarily on basal planes (Tullis *et al.* 1973).

Recrystallized grains. In order to obtain LPOs for quartz aggregates fully recrystallized in regime 1, we analyzed a fine-grained (diameter ~2 μm) novaculite sample shortened by 45%. The deformed sample has small (1–2 μm) polygonal grains with varying dislocation densities (Fig. 3c), similar to the recrystallized grains developed in quartzites deformed at the same conditions (Fig. 3b). Because the starting and final grain sizes are almost identical, it is difficult to determine from the microstructures alone whether the sample is completely recrystallized, i.e. if all the original grains have been swept by grain boundaries. The grain boundary velocity data of Tullis & Yund (1982) indicate that at least half of the volume of the sample would have been swept by grain boundaries during static annealing at our experimental conditions. During deformation, however, the volume swept should be considerably larger due to the maintenance of large dislocation density gradients. Furthermore, the sample has reached steady-state flow stress (Hirth & Tullis 1992), indicating that is has steady-state microstructures and is fully recrystallized.

The *c*-axis profile for the completely recrystallized novaculite (Fig. 7b) contrasts in two ways with those for the non-recrystallized quartzites described above. First, the maximum is parallel to σ_1, rather than at 20°. Second, the profile for the recrystallized grains has a minimum at ~60° to σ_1 and increases to uniform density at 80–90°, whereas that for the non-recrystallized grains shows a steady decrease in density from 20° to 70° and remains below uniform density to 90°.

The differences in the LPOs for quartzites and novaculites deformed in regime 1 indicate that the inferred grain boundary migration recrystallization results in a different LPO than intracrystalline slip. We assume that the deformation of the novaculite sample occurs by slip on the same basal and prism slip systems active in quartzites deformed at the same conditions. Thus grain boundary migration recrystallization is altering the LPO that is produced by intracrystalline slip. The observed increase in volume of grains with *c*-axes oriented parallel to σ_1 indicates that these grains are favored for growth. This in turn suggests that these 'hard' grains, poorly oriented for basal or prism *c*-slip, have lower dislocation densities than grains of 'softer' orientations. This is consistent with previous observations that less deformed augen in highly strained quartzites have their *c*-axes parallel to σ_1 (Tullis *et al.* 1973, Law 1986).

Regime 2: subgrain rotation recrystallization

Dislocation creep in regime 2 occurs at higher temperatures and slower strain rates than in regime 1, and diffusion-controlled dislocation climb is rapid enough to accommodate recovery (Hirth & Tullis 1992). At the optical scale, non-recrystallized grains are homogeneously flattened and show smooth undulose extinction, deformation lamellae and subgrains. Recrystallized grains form a mantle around the non-recrystallized grains (e.g. White 1976) (Fig. 4a). At the TEM scale, evidence for climb includes low densities of curved free

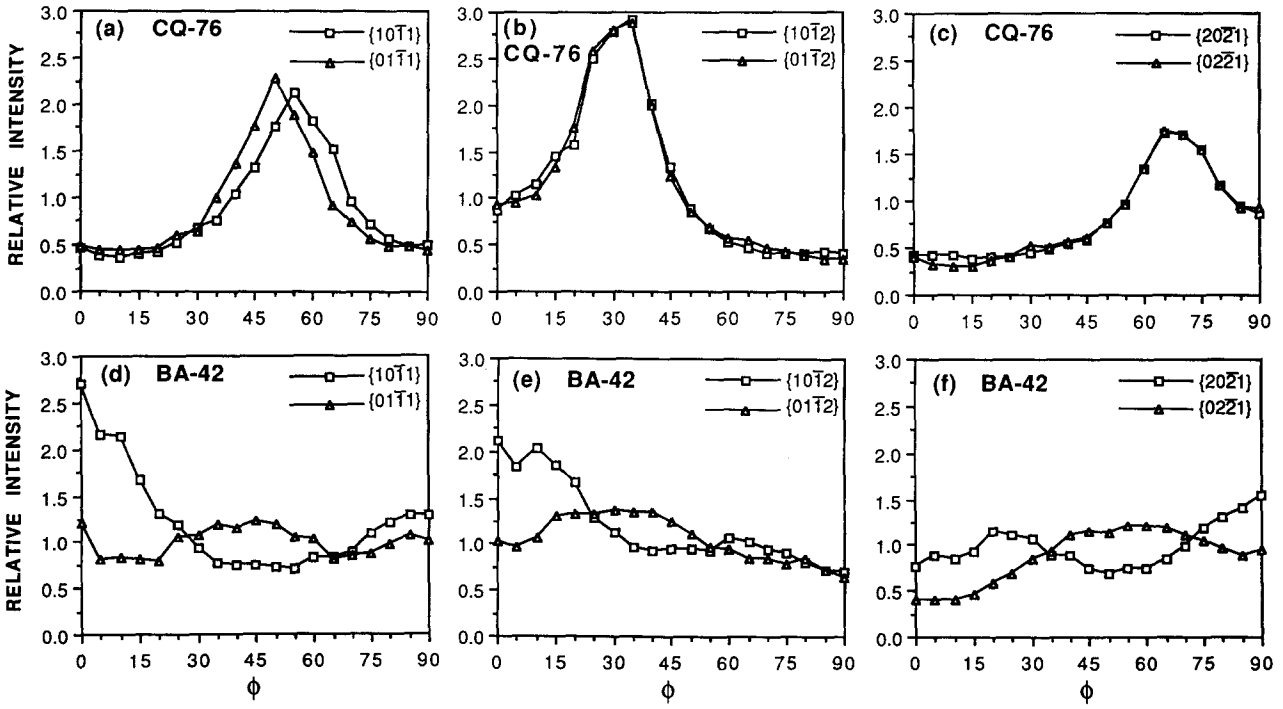

Fig. 2. Contribution of positive and negative forms to the scans of {10$\bar{1}$1} + {01$\bar{1}$1}, {10$\bar{1}$2} + {01$\bar{1}$2} and {20$\bar{2}$1} + {02$\bar{2}$1} for samples CQ-76 (a–c) and BA-42 (d–f). Axes are the same as in Fig. 1.

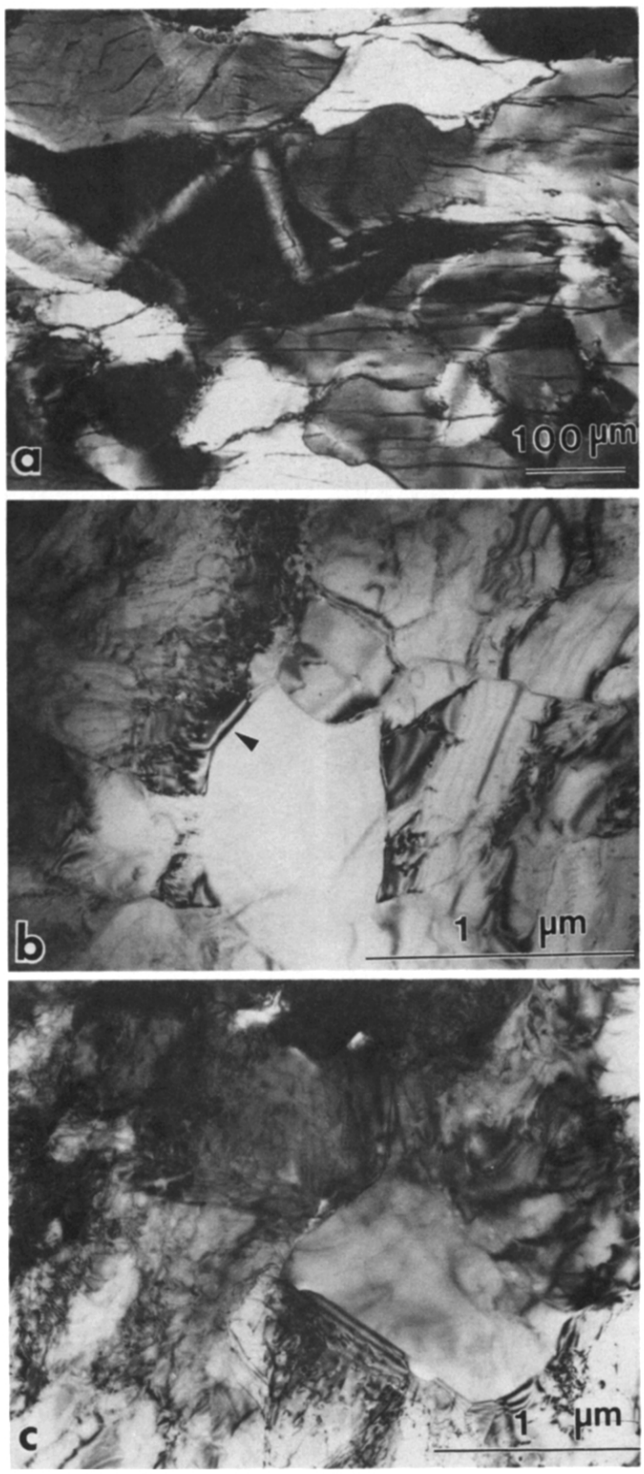

Fig. 3. Regime 1 microstructures. σ_1 is vertical in each photograph. Horizontal cracks are due to unloading after the experiment. (a) Non-recrystallized quartzite (W-340, 700°C, 10^{-6} s^{-1}, no added water, 20% ε). Optical photomicrograph. Note patchy extinction and deformation bands. (b) Partially recrystallized quartzite (GB-309, same conditions as above, 60% ε). TEM micrograph. Strain-free recrystallized grain with grain boundary convex towards grain with higher dislocation density (arrow). (c) Completely recrystallized novaculite (CQ-83, 750°C, 10^{-5} s^{-1}, 0.17 wt % water added, 45% ε). TEM micrograph. Strain-free grain surrounded by grains with higher dislocation densities.

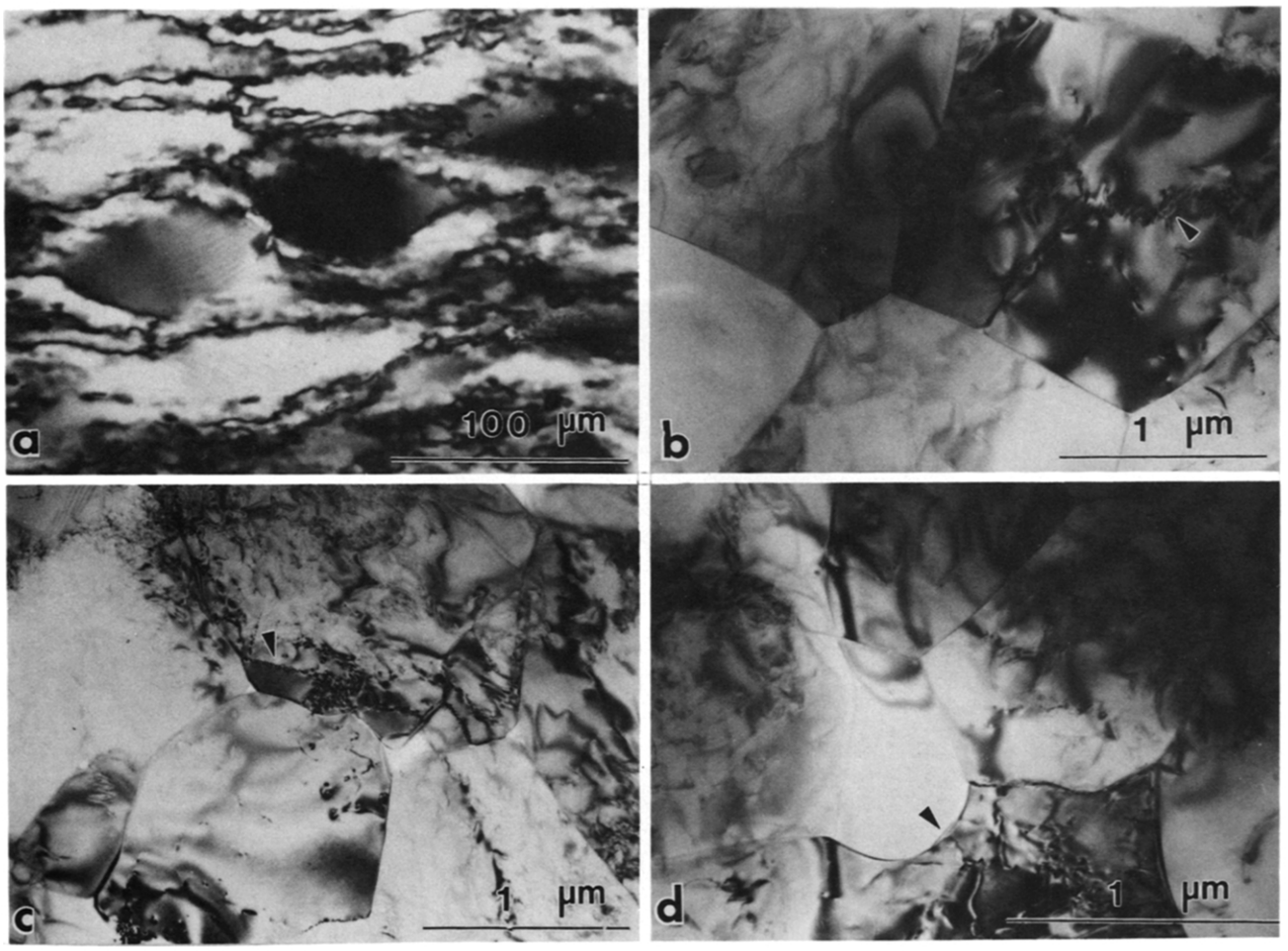

Fig. 4. Regime 2 microstructures. σ_1 is vertical in each photograph. (a) Partially recrystallized quartzite (BA-20; 800°C, 10^{-6} s^{-1}, 50% ε). Optical photomicrograph. Note subgrains and 'core and mantle' structure. (b) Partially recrystallized quartzite (AN-8; 800°C, 10^{-6} s^{-1}, 59% ε). TEM micrograph. Note low dislocation density, recrystallized grains and subgrain boundary (arrow). (c) Completely recrystallized novaculite (CQ-94; 700°C, 10^{-6} s^{-1} strain rate, 0.16 wt % water added, 55% ε). TEM photomicrograph. Note equant recrystallized grains and subgrain boundary (arrow). (d) Completely recrystallized novaculite (NV-53; 850°C, 10^{-6} s^{-1}, 0.03 wt % water added, 58% ε). TEM photomicrograph. Note strain-free recrystallized grain with grain boundary convex towards grain with higher dislocation density (arrow).

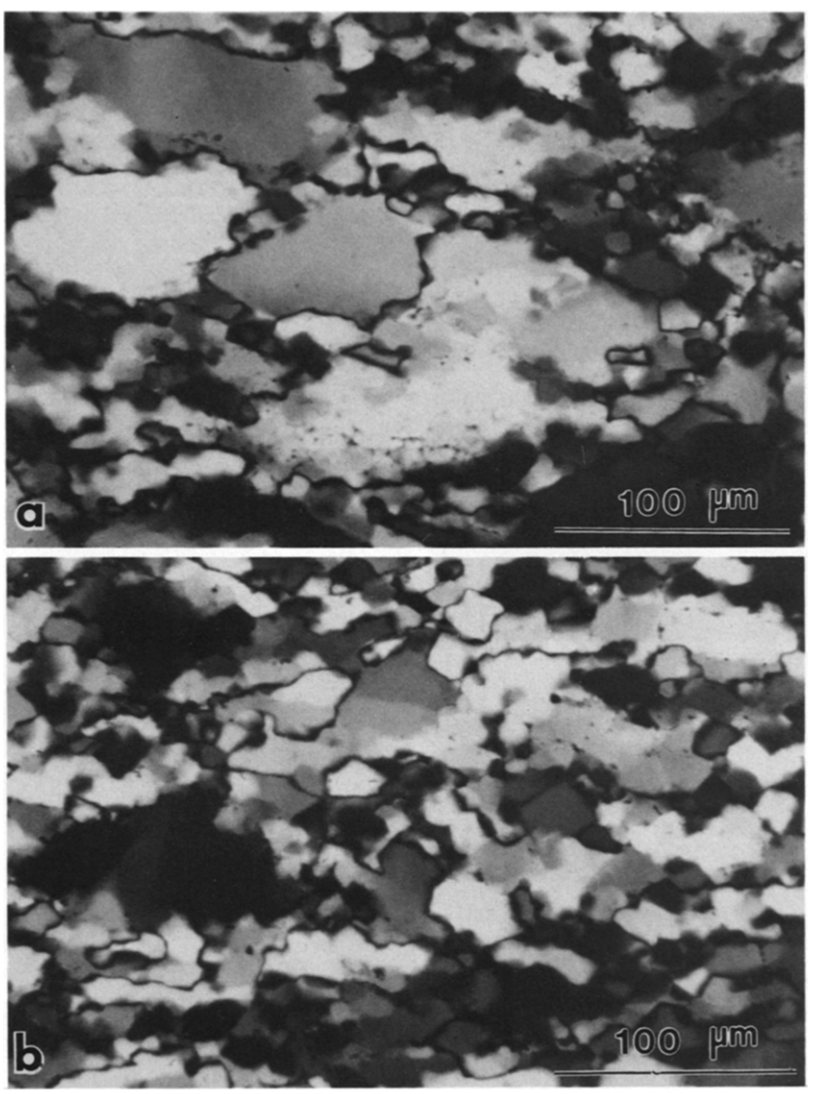

Fig. 5. Regime 3 microstructures. σ_1 is vertical in each photograph. (a) Partially recrystallized quartzite (CQ-78; 900°C, 10^{-6} s^{-1}, 0.16 wt % water added, 37% ε). Optical photomicrograph. Note straight grain boundaries and large subgrains. (b) Completely recrystallized quartzite (BA-42, 900°C. 10^{-6} s^{-1}, 0.16 wt % water added, 50% ε). Optical photomicrograph. Note weak horizontal foliation.

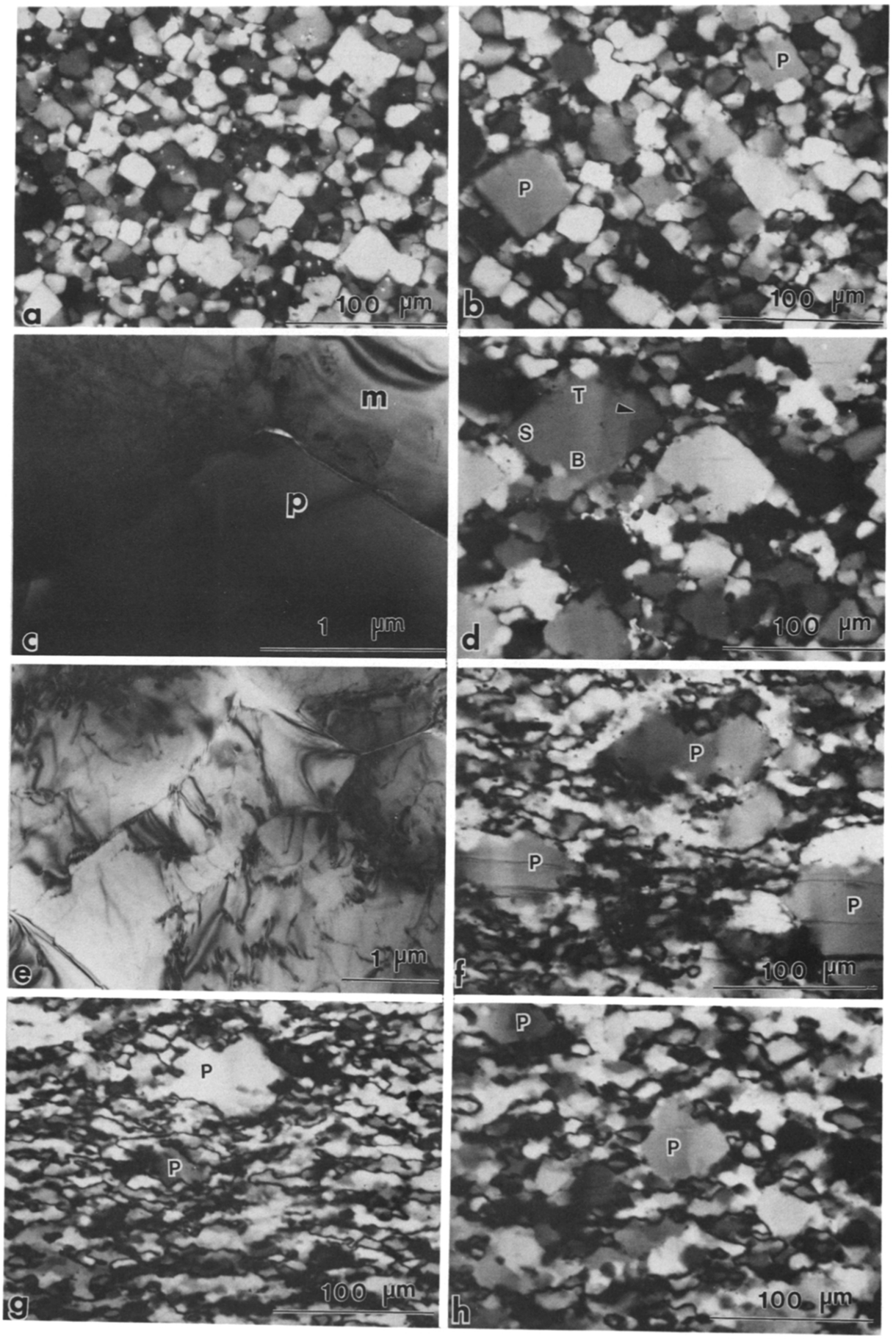
a
100 μm
b
P
P
100 μm
c
m
p
1 μm
d
T
S
B
100 μm
e
1 μm
f
P
P
P
100 μm
g
P
P
100 μm
h
P
P
100 μm

Fig. 6.

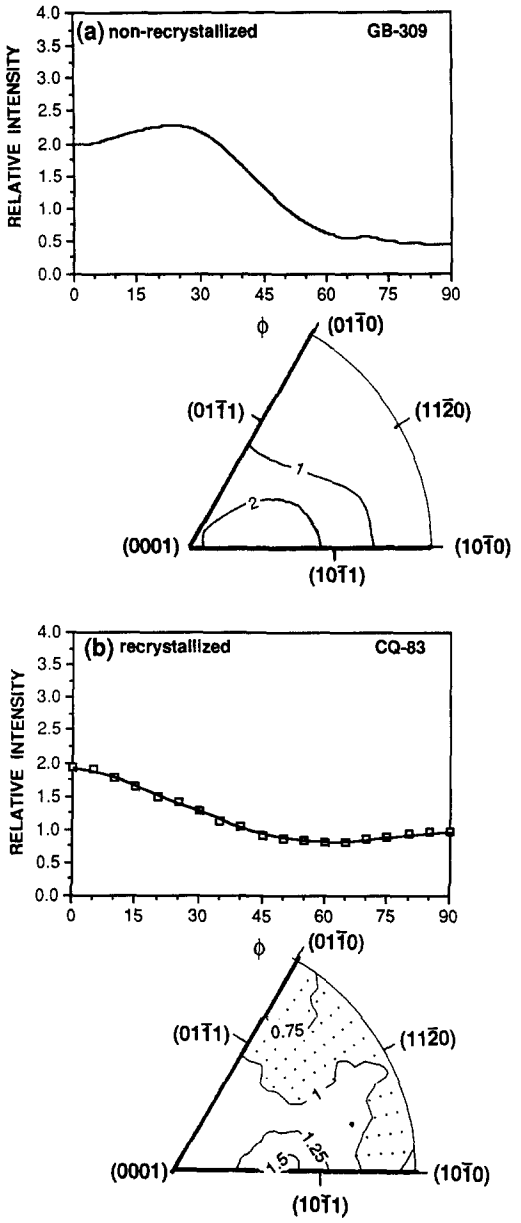

Fig. 7. *c*-axis profiles (pole density vs angle ϕ from σ_1) and inverse pole figures (the distribution of the σ_1 axis with respect to the crystal co-ordinates contoured in multiples of uniform distribution) for regime 1. (a) Non-recrystallized quartzite (GB-309; 700°C, 10^{-6} s^{-1}, 60% ε, ~7% recrystallized). (b) Completely recrystallized novaculite (CQ-83; 750°C, 10^{-5} s^{-1}, 0.17 wt % water added, 45% ε). Stippled area of inverse pole figure indicates relative intensity less than uniform.

dislocations and subgrain boundaries (Fig. 4b). Dynamic recrystallization occurs by progressive subgrain rotation. As more dislocations of one sign glide and climb into the subgrain boundaries, adjacent subgrains become increasingly misoriented with respect to one another and the boundary becomes a high-angle grain boundary at ~10° (e.g. White 1976). The new grains that form by this process are of a size similar to the subgrains. The recrystallized grains also have dislocation densities similar to their 'parent grain', resulting in similar strengths. Thus samples reach mechanical steady-state at very low strain, long before complete recrystallization (Hirth & Tullis 1992).

Non-recrystallized grains. We determined the *c*-axis LPOs of non-recrystallized grains in quartzite samples deformed over a range of temperatures and strain rates (see Table 1). With increasing temperature or decreasing strain rate within this regime, there is a reduction in the number of grains with deformation lamellae, a decrease in the free dislocation density and an increase in the volume of recrystallized grains at a given sample strain.

The *c*-axes of non-recrystallized grains were measured on a universal stage for samples shortened 50%. At lower temperatures within this regime, the non-recrystallized grains develop a small-circle girdle at 25–35° (ϕ) from σ_1 (Figs. 8a & b). Previous work demonstrated that with increasing strain at identical conditions, the opening angle of the girdle does not change, although the intensity strengthens (Tullis 1971). Quartzites deformed at higher temperatures in this regime develop essentially the same pattern (Figs. 8c & d), demonstrating that there is no abrupt change in the LPO corresponding to the α–β transition (Gleason & Tullis 1989). This observation is consistent with previous work on single crystals of synthetic quartz which suggests that the slip systems active in α- and β-quartz are essentially the same (e.g. Baeta & Ashbee 1969a,b, Blacic 1975, Kirby 1977, Linker *et al.* 1984).

Recrystallized grains. The recrystallized grains in the deformed quartzites continue to deform by slip, as suggested by the development of subgrain boundaries within them (Fig. 4b). However, they maintain their equant shape during subsequent deformation indicating that their boundaries migrate somewhat as deformation continues.

We have not been able to directly measure the LPO of the recrystallized grains in the quartzites. They are too small (2–10 μm, depending on the deformation temperature and thus applied stress) to measure on a universal stage, and because the samples are not completely recrystallized the LPO measured by X-ray goniometer methods includes a significant contribution from the non-recrystallized grains. Some constraints on the LPO

Fig. 6. (a)–(g) Micrographs of deformed flint, illustrating the microstructural evolution with increasing strain. All samples deformed at 900°C, 10^{-5} s^{-1}. σ_1 is vertical in all micrographs. (a) BA-30, 20% ε. Optical photomicrograph of square porphyroblasts. Bright specks are calcite. (b) BA-26, 30% ε. Optical photomicrograph. Porphyroblasts (P) have increased in size. (c) BA-26, TEM micrograph showing dislocation density contrast between matrix grain (m) and porphyroblast (p). (d) BA-51, 52% ε. Optical photomicrograph showing subgrain boundaries parallel to σ_1 (arrow). Note top (T) and bottom (B) 'corners' of porphyroblasts are not as well developed as side (S) 'corners'. (e) CQ-76, 48% ε, TEM micrograph of matrix grains. (f) BA-21, 60% ε. Optical photomicrograph. Note top and bottom corners of porphyroblasts (P) are recrystallized. Horizontal cracks are due to unloading after the experiment. (g) BA-25, 75% ε. Optical photomicrograph. Note there are only a few porphyroblast remnants (P). (h) Optical photomicrograph of completely recrystallized novaculite (CQ-84; 900°C, 10^{-6} s^{-1}, 0.17 wt % water added, 57% ε) for comparison. Note rhombic-shaped 'porphyroblasts' (P).

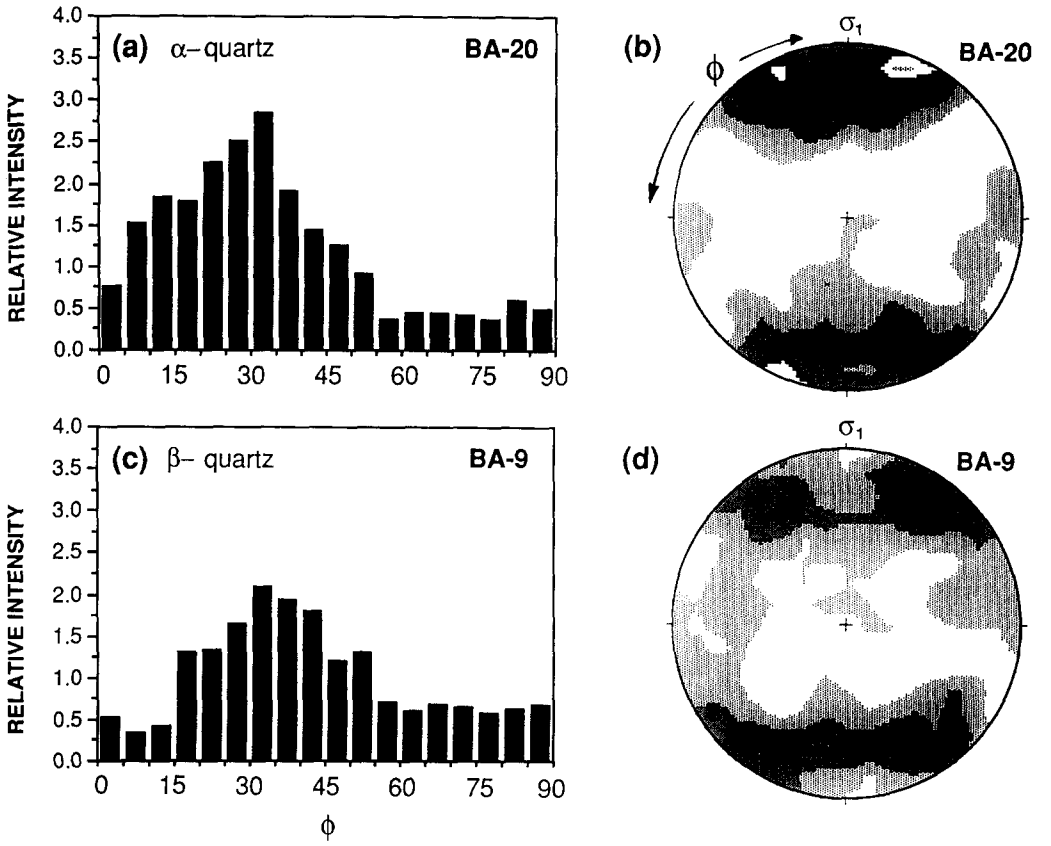

Fig. 8. *c*-axis profiles and pole figures for non-recrystallized quartzites deformed in regime 2. (a) & (b) α-quartz stability field (BA-20; 800°C, 1.02 GPa, 10^{-6} s^{-1}, 50% ε). Three hundred and fifty grains were measured on a universal stage. (c) & (d) β-quartz stability field (BA-9; 1100°C, 0.90 GPa, 10^{-5} s^{-1}, 50% ε). Five hundred grains were measured on a universal stage. Pole figures were contoured by the Kamb method. Contour intervals are two standard deviations.

of the recrystallized grains can be obtained by comparing the X-ray *c*-axis profiles of two quartzite samples deformed by Tullis (1971) in the β-quartz stability field at 900°C, 10^{-6} s^{-1}; one was shortened 50% (~40% recrystallized) and the other was shortened 75% (~60% recrystallized). The strength of the small-circle girdle increases with additional strain and recrystallization, but the opening angle remains the same (compare Figs. 9a & b). Although we cannot separate the effects of increased strain and increased recrystallization on the strengthening of the LPO, it is clear that the recrystallization does not change the LPO of the aggregate. This is reasonable because progressive subgrain rotation recrystallization produces grains that are initially misoriented from the original grain by only ~10°, and they reflect the most strained and rotated portions of the grains (White 1976). The new grains continue to deform on the same slip systems active in the 'parent' grains, and thus their orientation continues to evolve in a manner similar to that of the non-recrystallized grains.

We did not analyze the LPOs of grains recrystallized by progressive subgrain rotation in the α-quartz stability field. However, because the α–β transition does not affect the active slip systems in the non-recrystallized grains, and because the recrystallized grains have the same LPO as the non-recrystallized grains, we predict that the α–β transition will not have an effect on the LPO of recrystallized grains in this regime.

In order to determine the LPO of quartz aggregates completely recrystallized in regime 2, we analyzed two experimentally deformed novaculite samples. The deformed novaculite was intended to represent high strain, completely recrystallized quartzite; however, there is a possible problem with this analogy. The novaculites have a random LPO at the beginning of the deformation and recrystallization history, whereas quartzites undergo slip and develop an LPO before beginning to recrystallize. Thus, the recrystallized grains in the quartzite develop from grains already well oriented, whereas the recrystallized grains in the novaculite develop from randomly oriented material.

One of the novaculite samples was shortened 55% in the higher stress portion of regime 2 (700°C, 10^{-6} s^{-1}, 0.17 wt % water added). Because the initial grain size of the novaculite (2 μm) was close to the steady-state recrystallized grain size (2–3 μm), the novaculite was completely recrystallized after relatively low strain. Steady-state flow was reached by 10% shortening; we infer that the sample had a steady-state microstructure by this point as well. Optically, the sample has a grain shape foliation. However, at the TEM scale, equant recrystallized grains are present (Fig. 4c), indicating that grain boundary migration occurs in the novaculites just as in the quartzites (Fig. 4b). If no grain boundary migration occurred, then the recrystallized grains would have aspect ratios closer to that corresponding to the total sample strain.

The LPO of this completely recrystallized sample was

measured by X-ray goniometer methods. The *c*-axis profile shows a weak, broad maximum extending from 0° to 35° to σ_1 (Fig. 9c). This pattern is in contrast to the *c*-axis profiles for both the non-recrystallized grains and the recrystallized grains in the quartzites, which show small-circle girdles at 25–35° to σ_1 (Figs. 8a and 9a).

Another novaculite sample was shortened 58% in the lower stress portion of regime 2 (850°C, 10^{-6} s^{-1}, 0.03 wt% water added). Because the initial grain size of the novaculite sample (4 μm) was close to the steady-state recrystallized grain size, the sample was completely recrystallized and had reached steady-state flow after relatively low strain (Hirth & Tullis 1992). Optically, this sample also shows a grain shape foliation, although it is weaker than that found in the novaculite deformed at lower temperature. The recrystallized grains average 7 μm in diameter, indicating that some grain growth has occurred. The free dislocation density observed in TEM is similar to that observed in quartzite samples deformed in regime 2 (Figs. 4b & d). However, there is more variation in dislocation density from grain to grain than found in the quartzites, and evidence for local strain-induced grain boundary migration (Fig. 4d).

The LPO of this completely recrystallized sample was measured by X-ray goniometer methods. The *c*-axis profile has two components: a *c*-maximum and a small-circle girdle at 35–40° to σ_1 (Fig. 9d). This is in contrast to the *c*-axis profiles of the non-recrystallized grains and the recrystallized grains in quartzites deformed at comparable conditions, which show only a small-circle girdle at ~40° to σ_1 (Figs. 8b and 9a & b). We interpret the *c*-maximum component to be due to grain boundary migration and the small-circle girdle component to be due to intracrystalline slip.

The LPO data for the quartzites and novaculites suggest that the difference in the initial grain sizes results in different LPOs. Although the recrystallized grains in both the quartzites and the novaculites show evidence for grain boundary migration, only the novaculite developed the *c*-maximum component which we have attributed to grain boundary migration. We believe this is because the novaculites have a random LPO at the beginning of their deformation history, and thus have a number of grains oriented with their *c*-axes parallel to σ_1 which can grow at the expense of the other grains, and contribute a *c*-maximum component to the LPO. The quartzite did not develop a *c*-maximum because the small recrystallized grains which undergo grain boundary migration originate with their *c*-axes at ~30–40° to σ_1. Thus when the quartzite becomes sufficiently fine grained for grain boundary migration to sweep across a significant volume per unit time, few recrystallized grains are oriented favorably for growth.

Regime 3: *high-temperature grain boundary migration*

Dislocation creep in regime 3 occurs at higher temperatures and slower strain rates than in regime 2. Recovery is accommodated by dislocation climb, as in regime 2, but grain boundary mobility is enhanced by the increased temperature. In quartzites, the recrystallized grains are *larger* than the subgrains, indicating rapid boundary migration. The dislocation densities of both the old grains and the recrystallized grains are homogeneous and low, and grain boundaries cusp into subgrain boundaries (Hirth & Tullis 1992). These two observations suggest that the driving force for grain boundary migration may be a reduction in the energy of subgrain boundaries rather than the energy of individual dislocations (Hirth & Tullis 1992). Quartzite samples are fully recrystallized after ≤50% strain, and the recrystallized grains are larger than those in regime 2. Although subgrains form, it is not clear how much of the recrystallization occurs by progressive subgrain rotation. Grains are more homogeneously deformed than those at lower temperatures, perhaps due to the operation of more slip systems, which would reduce the strain gradients and the tendency for subgrain rotation. As in regime 2, the samples reach mechanical steady state at very low strain (Hirth & Tullis 1992).

Non-recrystallized grains. Because samples are fully recrystallized by ~50% strain in this regime, we determined *c*-axis LPOs of non-recrystallized grains in a quartzite sample shortened 36% in the lower temperature (<1000°C) portion of regime 3. At this strain, original grains have a core and mantle structure with optically visible subgrains which are larger than those seen in regime 2 (compare Figs. 4a and 5a). The non-recrystallized grains are less flattened than those in regime 2 samples shortened the same amount, due to the greater rate of grain boundary migration (Fig. 5a).

The *c*-axis LPO of the non-recrystallized grains was measured on the universal stage. The *c*-axis profile shows a broad small-circle girdle centered at 30° to σ_1 with a density of about twice a uniform distribution (Fig. 10a). This profile is not very different from that of non-recrystallized grains in quartzite shortened a similar amount in regime 2 (Fig. 10b), suggesting that similar slip systems are controlling the LPO. However, we cannot determine the *c*-axis LPO of non-recrystallized grains at higher temperatures within regime 3, where we might expect a transition to dominantly prism slip (e.g. Mainprice *et al.* 1986).

Recrystallized grains. The LPOs of completely recrystallized quartzites (50% strain) were determined from X-ray goniometer methods. At lower temperatures (≤1000°C) within this regime, the *c*-axis LPO is a small-circle girdle at about 45° to σ_1 with a density of about twice uniform distribution (Fig. 11a). The difference in ϕ between this recrystallized sample and the non-recrystallized grains in the sample discussed above may be explained by preferential recrystallization of grains favorably oriented for slip (Hippertt & Borba 1992). The grains oriented with their *c*-axes at 45° to σ_1 before deformation were probably recrystallized by 36% strain, and thus not included in the LPO of the non-recrystallized grains. The LPO of quartzite deformed at higher temperatures within regime 2 (Fig. 8b) and the LPO of

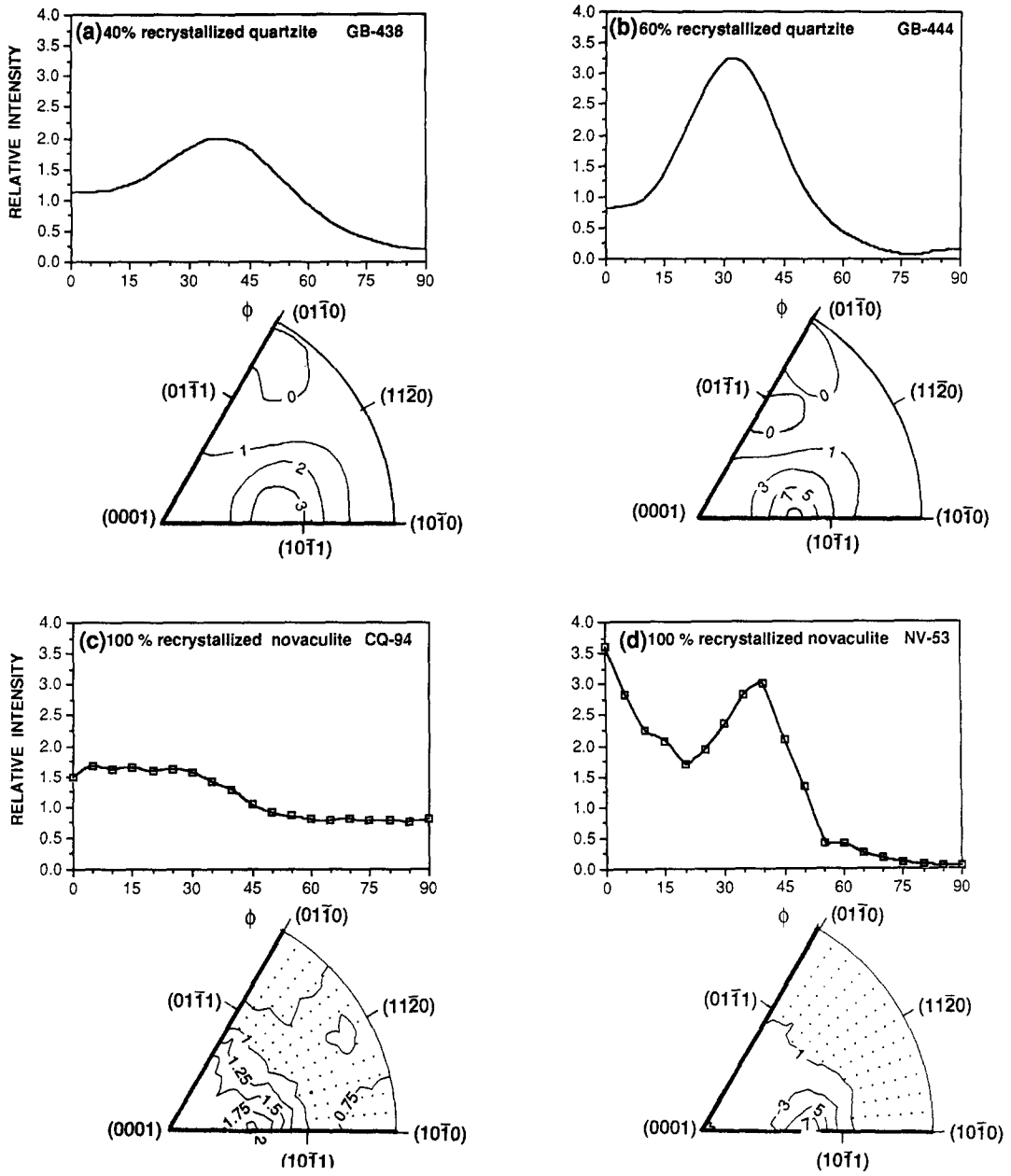

Fig. 9. *c*-axis profiles and inverse pole figures (contoured in multiples of uniform distribution) for aggregates recrystallized in regime 2. (a) & (b) Partially recrystallized quartzites. (a) GB-438; 900°C, 10^{-6} s^{-1}, 50% ε, 40% recrystallized. (b) GB-444; 900°C, 10^{-6} s^{-1}, 75% ε, 60% recrystallized. Note the similarity of the position of the peaks indicating that increased recrystallization does not affect the LPO. (c) & (d) Completely recrystallized novaculite. (c) CQ-94; 700°C, 10^{-6} s^{-1}, 0.17 wt % water added, 55% ε. (d) NV-53; 850°C, 10^{-6} s^{-1}, 0.03 wt % water added, 58% ε. Stippled area of inverse pole figures indicate relative intensity less than uniform.

the non-recrystallized grains in the quartzite sample deformed to lower strain within regime 3 (Fig. 10a) are both small-circle girdles. The similarity of these LPOs suggests that the girdle pattern produced by intracrystalline slip is not being preferentially removed by the more extensive grain boundary migration in regime 3. At higher temperatures in regime 3 (>1000°C), the *c*-axis profile still shows a small-circle girdle at about 45° to σ_1, but the density is only 1.5 times uniform (Fig. 11b). The weakening of the LPO may be due to the activation of additional slip systems at higher temperatures.

Although recrystallization in these samples occurs in part by grain boundary migration, the LPOs are not the same as those of novaculites recrystallized by grain boundary migration in regimes 1 and 2. We believe this is because grain boundary migration recrystallization in regime 3 is not driven by dislocation density gradients, which would favor grains poorly oriented for slip, but by reduction of surface energy (Hirth & Tullis 1992), which does not favor any particular orientation.

RESULTS II: RECRYSTALLIZATION DURING GRAIN GROWTH

The three dislocation creep regimes for quartz are based on microstructures that reflect different balances between the relative rates of dislocation production,

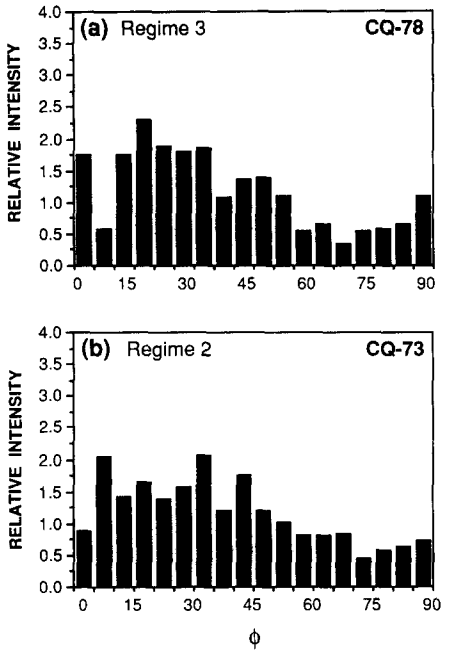

Fig. 10. (a) *c*-axis profile of non-recrystallized grains for quartzite deformed to low strain in regime 3 (CQ-78; 900°C, 10^{-6} s^{-1}, 0.16 wt % water added, 37% ε). (b) *c*-axis profile of non-recrystallized grains for quartzite deformed to low strain in regime 2 (CQ-73; 800°C, 10^{-6} s^{-1}, 30% ε). Three hundred grains were measured on a universal stage for each profile.

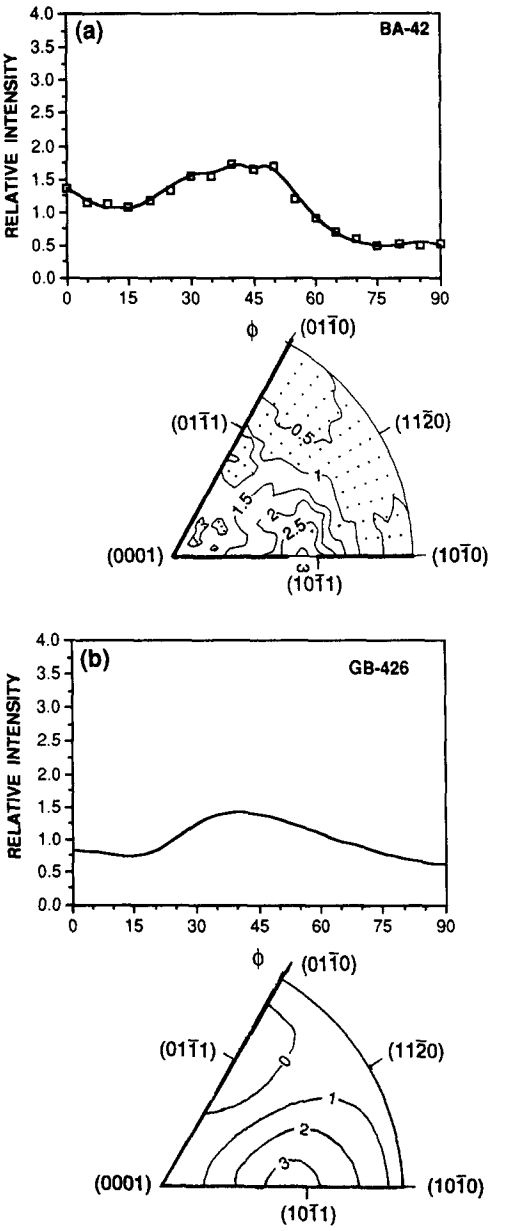

Fig. 11. *c*-axis profiles and inverse pole figures (contoured in multiples of uniform distribution) for quartzites recrystallized in regime 3. (a) BA-42; 900°C. 10^{-6} s^{-1}, 0.16 wt % water added, 50% ε. (b) GB-426; 1000°C, 10^{-7} s^{-1}, 76% ε. Stippled area of inverse pole figure indicates relative intensity less than uniform .

dislocation climb, and grain boundary migration (Hirth & Tullis 1992). However, when grain growth occurs in a fine-grained material, the rate of grain boundary migration can be higher than the rate of dislocation production and climb at least temporarily, as long as grain size remains small. In this section we document the LPOs of dynamically recrystallized grains developed during grain growth. Extremely fine-grained and 'wet' aggregates undergo rapid grain growth in the early stages of deformation, and develop microstructures and LPOs different from those which result from the recrystallization of coarser-grained aggregates deformed at the same conditions. However, with increasing strain, the grain growth ceases and both the microstructures and the LPOs gradually evolve to those characteristic of originally coarser-grained aggregates deformed at the same conditions. We illustrate this progression with experimentally deformed flint and novaculite samples (also listed in Table 1).

Flint

We deformed a series of flint samples (to 14, 20, 30, 48, 52, 60 and 75% strain, respectively) to document the evolution of LPOs and microstructures for the case in which grain growth rates are initially rapid. The very fine initial grain size (0.5–1 μm) of the flint results in a higher surface energy per volume than that in the quartzite samples. Because of this high surface energy and the high grain boundary mobility due to the large amounts of water present (1–2 wt %), grain growth begins as soon as the run temperature is achieved. Hydrostatic grain growth by itself produces no preferred orientation (Green *et al.* 1970, Mainprice 1981, Tullis & Yund 1982). However, under differential stress, grain boundary migration is influenced by dislocation density gradients, so grains of certain orientations are favored by growth, resulting in an LPO. Our series of flint experiments was carried out at conditions (900°C, 10^{-5} s^{-1}) that correspond to the high-temperature portion of regime 2 for quartzites with ~0.2 wt % water added. However, the relationship between the differential stress and strain is not like that of regime 2. In general, the stress increases gradually until about 40% strain and then gradually decreases with increasing strain (Fig. 12). We believe the transient strength can be correlated to the transient microstructures and LPOs the flint samples develop. We will first describe the sequence of microstructures and then the LPOs.

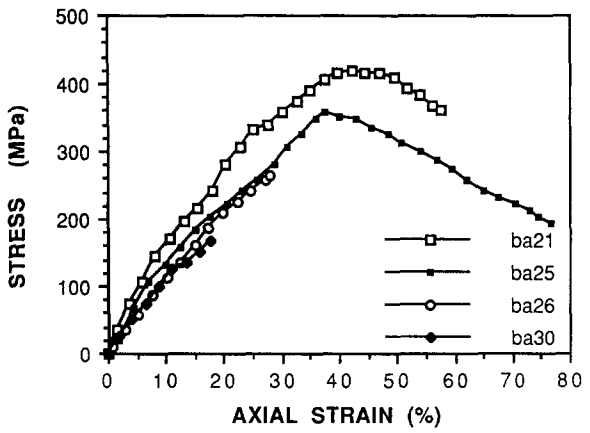

Fig. 12. Differential stress vs axial strain curves for flint samples deformed at 900°C, 10^{-5} s^{-1}, to various amounts of strain.

In our deformation experiments, there is a delay between when the run temperature (900°C) is achieved and when the advancing piston contacts the sample, initiating deformation. The piston displacement rate corresponding to a strain rate of 10^{-5} s^{-1} results in ~1.5 h of hydrostatic pre-heating. A sample from this stage of the experimental history has an average grain size of ~2–10 μm. There are a few larger (~15 μm) square porphyroblasts, which appear to have resulted from exaggerated grain growth. The angular relationship between the faces of these porphyroblasts and their *c*-axes indicates that the faces are $\{10\bar{1}1\}$ as noted previously by Green *et al.* (1970), and this has been confirmed in other studies by TEM (Mainprice & Paterson in press). The porphyroblasts and matrix grains are randomly oriented.

In a sample shortened 14%, the microstructures are very similar. The average grain size is ~4–15 μm, and a few square porphyroblasts have edges of ~20 μm. There is no optically discernible preferred orientation of the porphyroblasts or of the matrix, suggesting that at this point enhanced grain growth is driven mainly by the reduction of surface area.

In a sample shortened 20%, the average grain size is ~6–18 μm, and about 5% of the sample consists of square porphyroblasts with an edge length of ~20–40 μm (Fig. 6a). Many of these porphyroblasts are oriented with their *c*-axes within ~10° of σ_1; their edges are at 45° to σ_1, and their square corners line up parallel and perpendicular to σ_1 (Figs. 6b & d). TEM shows that the matrix grains contain curved dislocations, subgrain boundaries, and some twin boundaries. Some grains have dislocations that are perpendicular to the boundaries, consistent with rapid migration (Mainprice & Paterson in press). The porphyroblasts have *lower* dislocation densities than the matrix grains. One porphyroblast was observed to have a high dislocation density band in its center parallel to σ_1, and subgrain boundaries in the top and bottom corners, although the corners perpendicular to σ_1 have lower dislocation densities than the neighboring anhedral grains. Thus it appears that during the early strain history (<14% strain), grain growth is driven by the reduction of surface energy, producing porphyroblasts of all orientations; but by 20% strain the driving force for grain boundary migration has switched to dislocation density contrasts, resulting in the preferential growth of porphyroblasts oriented with their *c*-axes parallel to σ_1.

In a sample shortened 30%, square porphyroblasts of edge length ~40–60 μm constitute ~20% of the sample volume, and are set in a matrix of equant grains with an average diameter of ~8–20 μm (Fig. 6b). Almost all of the porphyroblasts are oriented with their *c*-axes within 10° of σ_1; a few have their *c*-axes perpendicular to σ_1 but these grains are fewer and smaller. Again, the porphyroblasts have lower dislocation densities than their neighbors (Fig. 6c). Because more of the sample volume consists of 'hard' porphyroblasts, and less of the sample volume is oriented favorably for easy slip, the sample strength increases (Fig. 12).

By approximately 50% shortening, many of the porphyroblasts have impinged in the σ_1 direction, due to their increased size (edge length ~50–120 μm) and the shortening strain (Fig. 6d). Deformation after impingement causes the porphyroblasts to develop optically visible subgrain boundaries subparallel to σ_1, and local undulatory extinction at their top and bottom corners. In some porphyroblasts, this has produced subgrain rotation recrystallization of the top and bottom corners (see labels in Fig. 6d). In contrast, the side corners of the porphyroblasts tend to remain sharp and unrecrystallized; thus many of the porphyroblasts are longer in the σ_2–σ_3 direction than they are in the σ_1 direction (Fig. 6d). The matrix grains, which constitute ~50% of the volume, are still mostly equant, with an average size of ~5–25 μm, and contain subgrain boundaries and varying dislocation densities (Fig. 6e). The impingement of the porphyroblasts correlates approximately with the peak strength on the stress–strain curve (Fig. 12), which occurs at ~40% strain. Beyond this point subgrain rotation recrystallization weakens the sample because it produces grains oriented favorably for slip.

A sample shortened 60% has a very different appearance, because it has a strong foliation (Fig. 6f). The matrix grains are smaller, due to subgrain rotation recrystallization of the former matrix grains as well as the margins of the porphyroblasts. In this foliated matrix, flattened 'regions' result from adjacent equant subgrains and recrystallized grains with similar orientations. Many of the porphyroblasts are oblate. They are shorter in the σ_1 direction than those in the samples shortened ~50%, due to increased recrystallization on the top and bottom corners (see labels in Fig. 6d), although some still have square side corners, indicating continued growth in the σ_2–σ_3 direction (Fig. 6f). Most of the porphyroblasts exhibit strong undulatory extinction, with optical subgrain boundaries parallel to *c*. Development of these subgrains can also be observed at the TEM scale. Subgrain rotation recrystallization is evident optically on the edges of many of the porphyroblasts (Fig. 6f). The recrystallized grains have *c*-axes rotated away from σ_1 relative to the orientation of the porphyroblast center; thus recrystallized grains on the

northwest and southeast edges have their *c*-axes rotated counter-clockwise, while those on the northeast and southwest edges have their *c*-axes rotated clockwise, relative to the host. These rotations result in part from the shearing of matrix grains past the inclined faces of the porphyroblasts.

In a sample shortened 75%, there are only a few remnants of porphyroblasts, set in a strongly foliated fine-grained (5–10 μm) matrix (Fig. 6g). The porphyroblast remnants again show strong undulatory extinction at their edges, leading into subgrains and recrystallized grains whose *c*-axes are rotated ~35° (clockwise on the northeast and southwest edges, counter-clockwise in the northwest and southwest edges). The porphyroblast remnants also have subgrain boundaries along prism planes forming long subgrains subparallel to σ_1 and recrystallized grains at the top and bottom corners. These recrystallized grains have diameters equal to the shortest dimension of the long subgrains, suggesting that they also formed by rotation from the subgrains. The average dislocation density of the matrix grains in this sample is similar to that found in quartzite samples with added water shortened 50% at the same conditions. The strength of the flint at this point approaches that of quartzite deformed under similar conditions in regime 2 (see Table 1).

The LPO changes progressively with the microstructures. At 14% shortening there is no optically detectable LPO. After only 30% shortening, however, the optically detectable LPO is fairly strong due to the alignment of the *c*-axes of most porphyroblasts (~20% of the sample volume) with the σ_1 direction. The LPO determined by X-ray goniometer methods shows a *c*-maximum parallel to σ_1 (Fig. 13a). After 48% shortening, the LPO is even stronger (Fig. 13b), reflecting the fact that the oriented porphyroblasts have grown to impingement in the σ_1 direction. This *c*-axis LPO is much stronger than any seen in quartzites experimentally shortened 50%. The deflection of the peak intensity from σ_1 by about 5° may reflect the misorientation of the subgrains in the porphyroblasts. After 60% shortening, the *c*-maximum LPO is still very strong (Fig. 13c). After 75% shortening, there are only a few remnants of porphyroblasts; the bulk of the sample is fine grained and strongly foliated. The *c*-axis profile for this sample shows a decreased intensity of the *c*-maximum (to 3.5 times a uniform density), and a subsidiary maximum or shoulder on the side of the main peak at about 30° to σ_1 (Fig. 13d). We believe this shoulder represents the development of a small-circle girdle due to intracrystalline slip. Thus the LPO as well as the microstructures and strength evolve toward those characteristic of steady-state flow in regime 2.

We have also deformed flint samples at other conditions to investigate how the grain growth rate and deformation rate compete to produce these microstructures and LPOs. Samples shortened 30 and 70% at 800°C and 10^{-5} s^{-1} had smaller porphyroblasts than samples shortened the same amounts at 900°C. This is consistent with a slower growth rate resulting from the lower temperature. The sample shortened 70% at 800°C had more porphyroblast remnants than the sample shortened the same amount at 900°C (Fig. 6g), suggesting that less subgrain rotation recrystallization after impingement had occurred in the 800°C sample. This is probably because the porphyroblasts grew more slowly and required higher strain for impingment than those in the 900°C samples.

We have also compared flint samples shortened the same amount (30%) at the same temperature (800°C), but at different strain rates. A sample deformed at 10^{-6} s^{-1} had larger porphyroblasts ($\leq$100 μm) than a sample deformed at 10^{-5} s^{-1} ($\leq$50 μm), presumably reflecting the order of magnitude longer time required for the same amount of shortening at the slower strain rate. This is consistent with growth rates of hydrostatically annealed flints (Tullis & Yund 1982).

Novaculite

Fine-grained novaculite samples deformed at temperatures $\geq$900°C with added water also undergo grain growth and develop LPOs with at least a component of *c*-axes parallel to σ_1. The amount of grain growth and the strength of the *c*-maximum component of the LPO depend on the amount of water present, the temperature and strain rate of deformation, and the initial grain size. Because novaculite has a larger initial grain size (2 μm) than flint, and less total water (0.17 wt % added water), the grain growth is less rapid in the novaculites at a given set of conditions.

A novaculite sample shortened 57% at regime 3 conditions (900°C, 10^{-6} s^{-1}, 0.17 wt % water added) has microstructures which are different than those of quartzites deformed in regime 3, but similar to those of the flint samples described above. The novaculite has large (~45 μm) square-shaped porphyroblasts with their *c*-axes parallel to σ_1, set in a matrix of smaller (3–20 μm) anhedral grains. Growth of the porphyroblasts plus axial shortening have lead to impingement, producing optically visible subgrain boundaries parallel to σ_1 and recrystallization at the top and bottom corners (Fig. 6h). Although slower strain rates tend to produce larger porphyroblasts, the porphyroblasts in this novaculite (shortened 57% at 10^{-6} s^{-1}) are shorter in the direction perpendicular to σ_1 than those in the flint shortened 52% at 10^{-5} s^{-1}. This slower growth rate is consistent with the lower water content and coarser initial grain size of the novaculite.

The LPO of the novaculite was determined by X-ray goniometer methods. The profile has a *c*-maximum parallel to σ_1, with a density of 12 times a uniform distribution (Fig. 13e). A completely recrystallized quartzite deformed at similar conditions developed a small-circle girdle at ~45° from σ_1 (Fig. 11a). The similarity of the microstructures and the LPO of this novaculite to those of the flint samples described above suggests that the LPOs for these fine-grained materials developed in the same way. Thus we would expect that

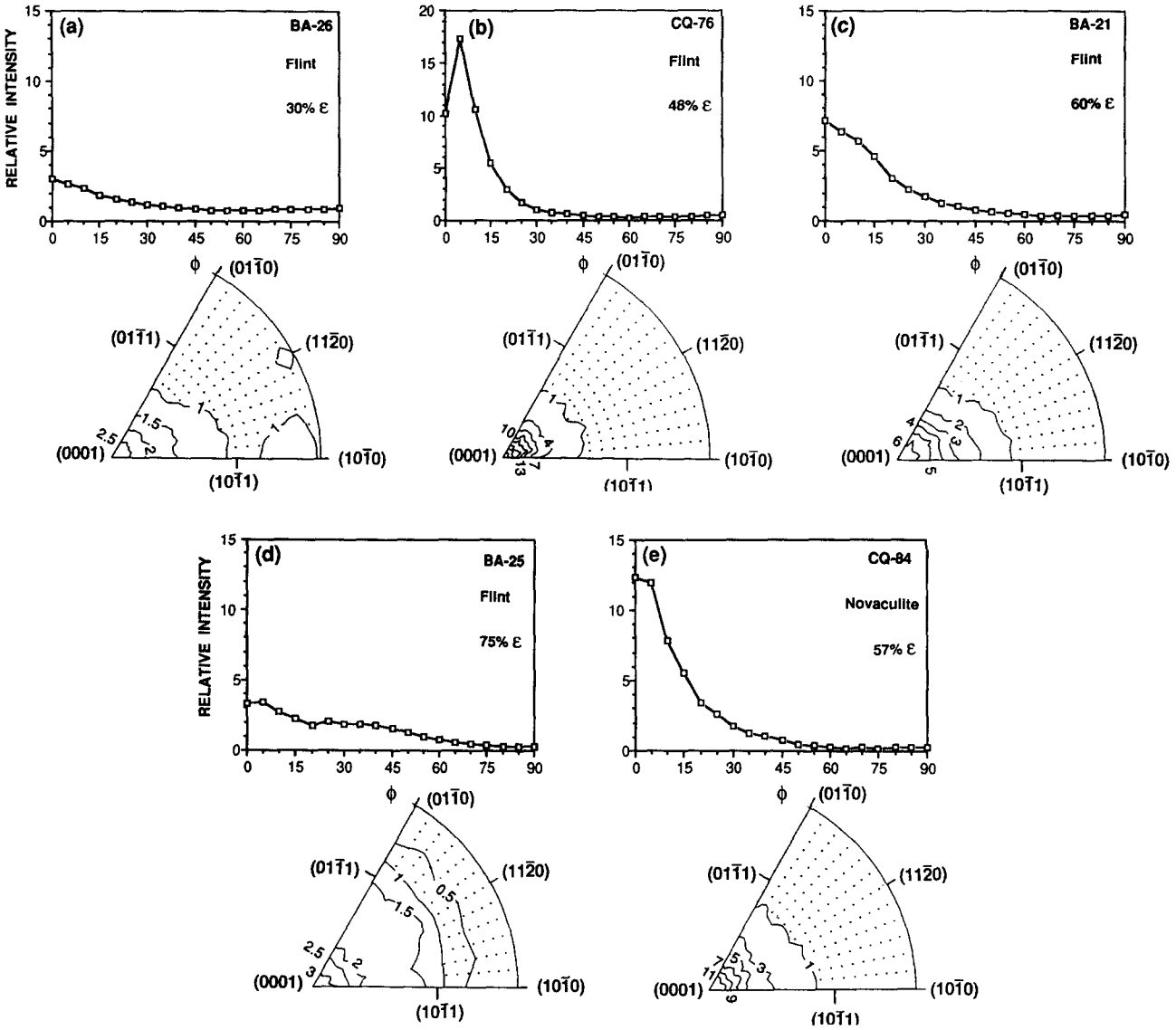

Fig. 13. *c*-axis profiles and inverse pole figures (contoured in multiples of uniform distribution) for fine-grained aggregates. Note the change in vertical scale from previous profiles. (a) Flint (BA-26: 900°C, 10^{-5} s^{-1}, 30% ε). (b) Flint (CQ-76: 900°C, 10^{-5} s^{-1}, 48% ε). Note again a change in vertical scale. (c) Flint (BA-21: 900°C, 10^{-5} s^{-1}, 60% ε). (d) Flint (BA-25: 900°C, 10^{-5} s^{-1}, 75% ε). (e) Novaculite (CQ-84; 900°C, 10^{-6} s^{-1}, 0.17 wt % water added, 57% ε). Stippled areas of inverse pole figures indicate relative intensity less than uniform.

with increasing strain the novaculite LPO would evolve into a small-circle girdle.

The microstructures and textures reported here are not restricted to the specific cases of flint and novaculite, but rather to 'wet' quartz aggregates of very fine initial grain size. They have also been observed in aggregates hot pressed from fragments (2–10 μm) of Brazil quartz and Black Hills quartzite, deformed 'as-is' (although with ~0.1 wt % adsorbed water) at 1.2 GPa and 900°C (Dell'Angelo unpublished results).

DISCUSSION

Summary: how dynamic recrystallization affects quartz LPOs

The LPOs of the non-recrystallized grains reported here are very similar to those reported by Tullis *et al.* (1973), namely a small circle girdle whose opening angle ranges from ~25° (Fig. 7a) to ~35° (Fig. 8). As pointed out by Tullis *et al.* (1973), these patterns are probably due to basal slip with increasing proportions of prism slip, consistent with the slip systems observed in experimentally deformed single quartz crystals (Baeta & Ashbee 1969a,b, Blacic 1975). No abrupt change in the LPO corresponding to the α–β transition was observed. This is consistent with previous work which suggests the slip systems active in α- and β-quartz are essentially the same (e.g. Baeta & Ashbee 1969a,b, Blacic 1975, Kirby 1977, Linker *et al.* 1984). Although we have presented the LPO data for non-recrystallized grains in the context of the three dislocation creep regimes (Hirth & Tullis 1992), it is clear that the LPOs of the non-recrystallized grains are independent of the operating recrystallization mechanism.

Our results show that the LPOs of dynamically recrystallized quartz aggregates depend on the dominant

mechanism of recrystallization, which fundamentally depends on the dominant mechanism of recovery: grain boundary migration recrystallization or dislocation climb. When recovery occurs dominantly by strain-induced grain boundary migration recrystallization, as it does in quartz aggregates deformed in regime 1, the resulting LPO of recrystallized grains is different than that of non-recrystallized grains. When recovery occurs dominantly by dislocation climb (leading to progressive subgrain rotation recrystallization), as it does in quartzites deformed in regime 2, the LPO of the recrystallized grains is similar to that of non-recrystallized grains. When recovery occurs by dislocation climb and grain boundary migration driven by surface energy reduction, as it does in quartz aggregates deformed in regime 3, the LPO is not altered by the recrystallization process. In wet, fine-grained aggregates, the rapid rate of grain boundary migration, due to the reduction of surface energy, combined with orientation dependent dislocation density contrasts allows the growth of grains oriented poorly for slip.

In regime 1, dislocation density gradients between grains of different orientations are large, resulting in a high driving force for grain boundary migration. Although grain boundary mobility is relatively low, the rate of grain boundary migration is relatively high, due to the high driving force. We interpret the *c*-maximum LPO of the recrystallized novaculite to indicate that grains oriented with their *c*-axes parallel to σ_1 are favored for growth. Because grain boundary migration recrystallization favors grains with lower stored energy, i.e. fewer dislocations (Sellars 1978), we conclude that these grains, which are oriented poorly for slip on base and prism planes, have lower dislocation densities than grains with other orientations. This hypothesis is supported by our observations of deformed flint, in which porphyroblasts have 'hard' orientations (low resolved shear stress on the base and prism slip systems) and have *lower* dislocation densities than grains with 'soft' orientations. Grain boundary migration thus causes 'hard' grains to replace 'soft' grains, leading to a maximum of *c*-axes parallel to σ_1. This pattern is very different than the small-circle girdle produced by slip in non-recrystallized grains at the same conditions of deformation.

In regime 2, higher climb rates result in more homogeneous dislocation densities, more homogeneous flattening of the original grains and subgrain formation. In quartzites subjected to increasing strain, the subgrains progressively misorient, producing recrystallized grains which inherit the small-circle girdle LPO of their host grains and which continue to re-orient by slip on the same slip systems. However, in both quartzites and novaculites, the recrystallized grains maintain an equant shape and therefore must undergo some grain boundary migration. We believe that it is this process which adds a *c*-maximum component to the LPO of novaculites. Quartzites do not develop a *c*-maximum component because grain boundary migration is not significant until a substantial volume of recrystallized grains have developed. Since these grains have orientations similar to those of their deformed host, few recrystallized grains have the 'hard' orientations required for preferred growth. We predict that the girdle LPO will persist with increasing strain. In contrast, the novaculites have a random LPO at the beginning of their deformation history, including many grains oriented with their *c*-axes parallel to σ_1 which will grow at the expense of other grains, forming the *c*-maximum component. At this time, our data are insufficient to predict the evolution of the LPO of novaculites with increasing strain.

In regime 3, grain boundary migration appears to be driven primarily by surface energy reduction (Hirth & Tullis 1992). In quartzites, subgrains form, but most of the recrystallized grains appear to result from migration of original boundaries. The LPO of recrystallized grains is the same as that of original grains deformed by slip, because the fast rate of recovery by dislocation climb removes any dislocation density gradients, or arranges dislocations into lower energy subgrain boundaries, before significant grain boundary migration occurs. Thus no particular orientation is favored for growth, and the LPO of the recrystallized grains is similar to that of non-recrystallized grains. We predict that this girdle LPO will persist with increasing strain.

For quartz aggregates in which the initial grain size is very fine, resulting in grain growth during deformation, the LPOs of dynamically recrystallized grains change with increasing strain. This is because the driving force for grain boundary migration is initially enhanced by the large surface energy allowing grains oriented poorly for slip to grow at the expense of the other grains. At least for fast experimental strain rates, these aggregates develop a transient, porphyroblastic microstructure and a corresponding transient *c*-maximum LPO and strain hardening. With increasing strain grain growth slows, the porphyroblasts impinge and the microstructures, LPO, and flow stress evolve toward those characteristic of the given deformation conditions. At these conditions, where dislocation density differences between grains of different orientations are very low, it seems somewhat surprising that the 'hard' orientation grains are so efficiently selected for growth. However, if grain boundary migration is very fast relative to the rate of dislocation climb, then small dislocation density gradients may exist long enough to influence the migration direction.

Comparison with other experimental studies on quartz aggregates

Ours is the first experimental study to investigate how dynamic recrystallization affects the LPO of quartz aggregates which undergo grain size reduction as well as grain growth (due to reduction in total grain surface area) during deformation. Several previous studies have used flint and novaculite as starting materials in order to 'speed up' the recrystallization process. Thus our comparisons with other experimental studies on quartz aggregates focus on flint and novaculite.

Deformation experiments on flint and novaculite

were conducted by Green *et al.* (1970) over a wide range of pressure and temperature, in order to study the LPOs produced by dynamic recrystallization, but sample strains were mostly ≤30%, and no TEM observations were made to determine the recrystallization mechanism. At low temperatures (<700°C at 10^{-5} s^{-1}) within the α-quartz field, the flint developed a *c*-maximum pattern, which they attributed to the preferential growth of grains with lower dislocation densities. This is consistent with our interpretation for novaculites deformed in regime 1. They found a transition from a *c*-maximum pattern to a small-circle girdle pattern with increasing temperature within the α-quartz field. They speculated that this was due to an increase in the homogeneity of dislocation densities with increasing temperature, leading to less grain boundary migration, allowing slip to influence the LPO. Finally, at even higher temperatures, they observed a transition back to a *c*-maximum pattern, associated with the growth of porphyroblasts. They correlated this with the α–β-quartz transition, but did not suggest a mechanism for this change.

In our flint experiments we see no evidence for a switch in the LPO of the recrystallized grains at the α–β-quartz transition, nor a restriction of square porphyroblasts to the β-quartz field. Our samples develop porphyroblasts and a *c*-maximum pattern, even within the α-quartz field, although porphyroblasts are better developed at higher temperatures. We did not observe the small-circle girdle pattern reported by Green *et al.* (1970), even for samples deformed at the same conditions (e.g. 800°C at 10^{-6} s^{-1}). A small-circle girdle component only developed at high strain (75%), after the porphyroblasts had impinged. The reason for this discrepancy is not clear. Impurities can inhibit grain boundary migration (Guillope & Poirier 1979) and we found in some flint samples, not included in this study, that the presence of calcite along the grain boundaries inhibits porphyroblast development. Thus, if the flint samples of Green *et al.* (1970) had more impurities than ours, grain boundary migration and porphyroblast development may have been inhibited, especially at the lower temperatures.

Flint samples were experimentally deformed at 0.3 GPa, 500–1000°C and at strain rates of 10^{-3} to 10^{-5} s^{-1} by Mainprice & Paterson (in press). Within the dislocation creep field (stresses >100 MPa), samples deformed at higher temperatures and strains (~30%) developed square porphyroblasts and a *c*-maximum LPO, consistent with our higher pressure results. They attributed this LPO to the growth of neighboring grains related by low energy Esterel twin boundaries (parallel to $\{10\bar{1}1\}$), rather than to the growth of low dislocation density 'hard' grains. We observed twins in some porphyroblasts, but not all, and they were not always parallel to the grain boundaries. Samples of agate (similar to flint in having a fine grain size of ~2 μm and a water content of 2–4%) were deformed by Kern (1977) and Masuda & Fujimura (1981). However, these authors did not determine recrystallization mechanisms or make systematic measurements of LPO.

Novaculite samples of a range of grain sizes were experimentally deformed by Kronenberg & Tullis (1984) as part of a study of the effect of grain size, pressure and water on the deformation of quartz aggregates. The *c*-axis LPOs for several of these samples were measured photometrically by Price (personal communication 1986). Samples with 0.4 wt % water added and shortened 30% at 700°C, 10^{-6} s^{-1}, and 1.5 GPa underwent grain growth, although no porphyroblasts developed. The samples have developed a broad *c*-maximum parallel to σ_1. The deformation conditions correspond to the higher stress portion of dislocation creep regime 2 (Hirth & Tullis 1992), where at comparable strain the LPO of non-recrystallized aggregates is a very weak small-circle girdle. Thus we infer that the *c*-maximum patterns were due to grain boundary migration as we have inferred for the regime 2 novaculite samples in our study.

We have demonstrated that flint and novaculite are not good analogues for quartzites because of the transient behavior of the LPO, the flow stress and the microstructures with increasing strain. Therefore, although these aggregates do offer some insight into the development of LPOs during recrystallization, caution must be used when extrapolating experimental data from these aggregates to coarser naturally deformed quartz aggregates.

Comparison with other materials

Friedman & Higgs (1981) were among the first to demonstrate that the LPOs produced by dynamic recrystallization could differ from those produced by slip, based on their experimental study of calcite aggregates deformed over a range of temperatures. Because their experiments were done in simple shear and because mechanical twinning is very important in calcite, it is difficult to compare their results with ours. A difference between LPOs in recrystallized and non-recrystallized grains was also found by Kunze & Ave'Lallemant (1981) in non-coaxial (extrusion and punching) deformation experiments on olivine aggregates. They interpreted their data to indicate that the LPOs of dynamically recrystallized grains are controlled by the principal stress directions, whereas the LPOs of the non-recrystallized grains are kinematically controlled.

In more recent coaxial experiments on olivine aggregates, Toriumi & Karato (1985) and Karato (1987, 1988) demonstrated that different LPOs were produced by different mechanisms of dynamic recrystallization. At higher temperatures Karato (1988) found that recrystallized grains resulted from progressive subgrain misorientation and had an LPO similar to that produced by slip in the deformed original grains. At lower temperatures he found that recrystallized grains formed by strain-induced grain boundary migration, with boundaries migrating into 'softer' grains which contained a higher dislocation density; this resulted in [010] axes oriented parallel to σ_1, consistent with the results of Kunze & Ave'Lallemant (1981). We find the same

behavior for quartz aggregates deformed in regimes 1 (lower temperature) and 2 (higher temperature). Karato (1988) did not observe an even higher temperature regime 3 type behavior where grain growth is rapid but not driven by dislocation density differences, nor did he investigate the behavior of very fine-grained and 'wet' aggregates to high strains, to see whether they develop a transient LPO due to growth.

Karato (1987) concluded that the LPO of recrystallized olivine grains is determined by the relative rates of deformation and grain growth. He stated that at lower temperatures where growth is faster (due to higher dislocation density contrasts and to a smaller activation energy for grain boundary migration than that for creep), the LPO reflects the state of stress, whereas at higher temperatures where the strain rate can be higher at a given applied stress, the LPO reflects the kinematic framework. In the latter case he meant that the slip plane would align with the shear plane of simple shear, and slip direction would align with the shear direction. However, Wenk & Christie (1991) point out that the development of an LPO by slip reflects differential rates of rotation for grains of different orientations, and that maxima in the pole figure correspond to orientations for which rotations are slowest.

Although quartz and olivine are similar in the sense that 'hard' grains have lower dislocation densities and grow preferentially during grain boundary migration recrystallization, the opposite tendency has been observed in some other materials. 'Hard' grains are observed to be replaced by grain boundary migration in experimentally deformed octochloropropane (Jessell 1986) and ice (Wilson 1986), and in experimentally deformed camphor Urai *et al.* (1980) observed a tendency for 'soft' grains to grow the fastest. However, different recrystallization mechanisms and dislocation creep regimes have not been identified in these materials, so it is difficult to know whether other minerals might show fundamentally different behavior from quartz and olivine.

Implications for models of LPO development

Most computer simulations of LPO development in quartz aggregates have been based on the effects of intracrystalline slip (e.g. Lister & Hobbs 1980, Etchecopar & Vasseur 1987, Wenk *et al.* 1989). The effects of dynamic recrystallization have only recently been incorporated into models. The three-dimensional geometrical model of Etchecopar & Vasseur (1987) assumed that each grain is periodically restored to its original polyhedral shape, without addressing how the orientation of the deformed grain may affect this 'recrystallization' process. Jessell (1986, 1988a,b) and Jessell & Lister (1990) have incorporated both progressive subgrain rotation and grain boundary migration recrystallization into their models of LPO development in quartz aggregates. Their assumption of homogeneous strain forced them to assume that there is a direct correlation between a high resistance to deformation and a high dislocation density, and thus that grains oriented poorly for slip will be removed by grain boundary migration recrystallization (as suggested by Schmid & Casey 1986, pp. 283–284). However, we find that quartz grains poorly oriented for slip have *lower* dislocation densities and are *favored* for growth, indicating the samples are experiencing homogeneous *stress*.

Jessell & Lister (1990) argued that significant grain boundary migration required relatively high temperatures to provide the necessary mobility, and that at these high temperatures quartz aggregates would undergo homogeneous strain. Hirth & Tullis (1992) have demonstrated that at experimental strain rates, grain boundary migration occurs at relatively low temperatures (e.g. 700°C at $10^{-6}\,s^{-1}$). Although grain boundary mobility is low at these conditions, the high dislocation density contrasts provide a large driving force for grain boundary migration. At these conditions, quartz does not deform homogeneously (Tullis *et al.* 1973, Hirth & Tullis 1992) and thus models assuming homogeneous strain may predict erroneous LPOs. For recrystallization-accommodated dislocation creep (regime 1), it may be more accurate to assume homogeneous *stress*, in which case the dislocation density of a grain should be *inversely* related to its resistance to deformation. Jessell & Lister's (1990) model should be more applicable to the deformation of quartzites in dislocation creep regime 2, where the strain is more homogeneous. Their model should be most applicable to the deformation of quartzites in dislocation creep regime 3, where the strain is very homogeneous and grain boundaries have high mobility. However, we find that grain boundary migration recrystallization *does not* favor specific orientations in quartzite at these conditions, probably because dislocation density differences play a lesser role in inducing grain boundary migration. It is difficult to make specific comparisons with Jessell & Lister's (1990) model predictions because they are all for the case of simple shear, whereas our samples were all coaxially deformed.

The series of flint experiments from our study illustrates how stress in a sample can change from homogeneous to heterogeneous with increasing strain and changing microstructures. At low strain, the sample experiences homogeneous stress. The stress is high enough to initiate slip in the grains oriented favorably for easy slip, but is not high enough to initiate slip in the grains oriented unfavorably for slip, that is those grains oriented with their c-axes parallel to σ_1. Thus these grains become porphyroblasts which grow until they impinge and subsequently form a stress-supporting framework. At this point, the stress reaches a maximum as the porphyroblasts begin to deform. The porphyroblasts undergo subgrain rotation recrystallization which produces grains with orientations similar to those of the matrix grains, allowing a switch to homogeneous strain.

We conclude that for quartz, at least, models assuming homogeneous strain will be moderately successful in predicting LPOs produced in recrystallized quartzites deformed in dislocation creep regimes 2 and 3. In contrast, our study indicates that models assuming

homogeneous stress should be more successful in predicting the LPOs produced by grain boundary migration recrystallization, in dislocation creep regime 1. In very fine-grained and 'wet' quartz aggregates, such as flint, the assumption of homogeneous stress or homogeneous strain will depend on the strain history of the rock.

Application to natural tectonites

There has been great debate among those who have studied naturally deformed and recrystallized quartz aggregates as to whether dynamic recrystallization tends to favor grains with 'hard' or 'soft' orientations. Most authors have suggested that grain boundary migration is more likely to replace grains with high internal strain energy (e.g. Knipe & Law 1987). However, some have concluded that the 'soft' grains (grains oriented well for slip) will be the ones with higher strain energy and hence will be replaced (e.g. Shelley 1971, Gapais & Barbarin 1986), whereas others have concluded that the 'soft' grains will be the ones with lower strain energy and hence will be favored for growth (e.g. Mancktelow 1987). It is very difficult to prove one or the other without making direct comparisons of dislocation densities, and even TEM observations may not provide a clear-cut answer due to complications after the deformation event of interest (e.g. Knipe & Law 1987). However, our experimental results indicate that it is the grains with the 'hard' orientations which are favored for growth by grain boundary migration in quartz, as was also found for olivine (Karato 1988).

There have been only a few studies which have attempted to measure the LPOs of non-recrystallized and of dynamically recrystallized grains in deformed quartz aggregates. Law (1986) has measured the *c*-axis LPOs of host and recrystallized grains in partially recrystallized quartzites deformed coaxially at greenschist grade. The recrystallization mechanism appears to be progressive subgrain rotation. In general, the LPOs of the recrystallized and deformed original grains have the same pattern (a small-circle girdle about *Z* for flattening strain, forming a connection through *Y* for plane strain), although the LPO of the recrystallized grains is somewhat more diffuse. In a similar study, Kirchener & Teyssier (1991) attributed differences between the *c*-axis LPO of porphyroclasts and that of recrystallized grains to a change in the incremental strain history. However, they re-measured the LPO of some of their samples using a more inclusive criterion for defining porphyroclasts and the LPO patterns became less distinct, such that the recrystallized grains have similar orientations to although somewhat more diffuse than the porphyroclasts (Kirchener & Teyssier 1992). The results of these two studies match well with our results for quartzite deformed in regime 2, where the LPOs of recrystallized grains are very similar to those of deformed original grains.

We are not aware of any reports in the literature of naturally deformed quartz aggregates which have been completely recrystallized in regime 1, where the recrystallization mechanism leads to an LPO which is different from that produced by slip. However, there may be some instances of initially very fine-grained aggregates (either fault gouge or chert, for example) which have experienced a significant component of grain growth accompanying deformation, thus leading to a strong *c*-maximum LPO. The almost undeformed chert described by Wenk & Kolodny (1968) which has a *c*-maximum parallel to the sedimentary loading direction might be an example of this.

In most naturally deformed and recrystallized quartz aggregates the deformation is non-coaxial so that the principal axes of stress and finite strain are different. What effect will this have on the LPOs of dynamically recrystallized quartz aggregates? In regimes 2 and 3 the LPOs of the recrystallized grains should remain essentially the same as those produced by slip within original grains, just as for coaxial deformation. In situations where the LPO is due to grain boundary migration, either in regime 1 or during the transient low strain deformation of a very fine-grained, 'wet' aggregate, we expect that the tendency for the growth of porphyroblasts of 'hard' orientations should not be so strong, as these would rotate into orientations more favorable for slip, as suggested by Tullis *et al.* (1973) and Law (1986). However, if the rate of grain boundary migration is faster than the rate of lattice rotation, then the LPO resulting from dynamic recrystallization will be quite different from that due to slip.

CONCLUSIONS

For axial compression experiments, we find that the LPO of dynamically recrystallized quartzites will depend on the mechanism of recrystallization. Strain-induced grain boundary migration recrystallization produces *c*-maximum LPOs, due to the preferential growth of grains that are oriented poorly for slip and thus have a lower strain energy (regime 1). In contrast, non-recrystallized grains in this regime develop a tight small-circle girdle of *c*-axes. At higher temperatures (regime 2), progressive subgrain rotation produces recrystallized grains with small-circle girdle LPOs inherited from their deformed non-recrystallized hosts. At still higher temperatures (regime 3), recrystallized grains result from progressive subgrain rotation coupled with rapid grain boundary migration (driven by surface energy reduction); they develop a weak small-circle girdle of *c*-axes similar to that produced in non-recrystallized grains. If the initial grain size is small compared to the steady-state grain size and the aggregate is 'wet', then the rate of grain boundary migration (or grain growth) may be large relative to the rate of climb and a transient LPO will develop due to the growth of grains oriented poorly for slip. This transient LPO evolves with increasing strain toward the LPO characteristic of the dislocation creep regime.

Models assuming homogeneous *stress* should be successful in predicting the LPOs produced in regime 1 by

strain-induced grain boundary migration recrystallization and in very fine-grained aggregates (i.e. flint deformed in regime 2). Models assuming homogeneous *strain* should be moderately successful in predicting LPOs produced by progressive subgrain rotation recrystallization (i.e. quartzites deformed in regime 2). However, at higher temperatures where grain boundary migration (driven by surface energy reduction) also occurs (i.e. quartzites deformed in regime 3) grain boundary migration does not appear to favor specific orientations.

Acknowledgements—Supported by National Science Foundation Grant EAR-8917347. We thank B. Collins for thin sections of all types, G. Hirth and R. A. Yund for helpful discussions, G. Hirth, H.-R. Wenk and R. A. Yund for comments on the manuscript, and R. D. Law and S. Karato for constructive reviews.

REFERENCES

Ave'Lallemant, H. G. 1975. Mechanisms of preferred orientation of olivine in tectonite peridotite. *Geology* **3**, 653–656.

Ave'Lallemant, H. G. & Carter, N. L. 1971. Pressure dependence of quartz deformation lamellae orientations. *A. J. Sci.* **270**, 218–235.

Baeta, R. D. & Ashbee, K. H. G. 1969a. Slip systems in quartz: I. Experiments. *Am. Miner.* **54**, 1551–1573.

Baeta, R. D. & Ashbee, K. H. G. 1969b. Slip systems in quartz: II. Interpretation. *Am. Miner.* **54**, 1574–1582.

Baker, D. W., Wenk, H.-R. & Christie, J. M. 1969. X-ray analysis of preferred orientation in fine-grained quartz aggregates. *J. Geol.* **77**, 144–172.

Blacic, J. D. 1975. Plastic deformation mechanisms in quartz: the effect of water. *Tectonophysics* **27**, 271–294.

Dell'Angelo, L. N. & Tullis, J. 1989. Fabric development in experimentally sheared quartzites. *Tectonophysics* **169**, 1–21.

Etchecopar, A. & Vasseur, G. 1987. A 3-D kinetic model of fabric development in polycrystalline aggregates: Comparisons with experimental and natural samples. *J. Struct. Geol.* **9**, 705–717.

Friedman, M. & Higgs, N. G. 1981. Calcite fabrics in experimental shear zones. *Am. Geophys. Un. Geophys. Monogr.* **24**, 11–27.

Gapais, D. & Barbarin, B. 1986. Quartz fabric transition in a cooling syntectonic granite (Hermitage Massif, France). *Tectonophysics* **125**, 357–370.

Gleason, G. C. & Tullis, J. 1989. *c*-axis preferred orientations of quartzites deformed and annealed in the alpha and beta quartz fields. *Trans. Am. Geophys. Un.* **70**, 458.

Green, H. W., II, Griggs, D. T. & Christie, J. M. 1970. Syntectonic and annealing recrystallization of fine-grained quartz aggregates. In: *Experimental and Natural Rock Deformation* (edited by Paulitsch, W.). Springer, Berlin, 272–335.

Guillope, M. & Poirier, J. P. 1979. Dynamic recrystallization during creep of single-crystalline halite: an experimental study. *J. geophys. Res.* **84**, 5557–5567.

Hippertt, J. F. M. & Borba, R. P. 1992. Quartz *c*-axis fabric differences between porphyroclasts and recrystallized grains: Discussion. *J. Struct. Geol.* **14**, 627–630.

Hirth, G. & Tullis, J. 1992. Dislocation creep regimes in quartz aggregates. *J. Struct. Geol.* **14**, 145–159.

Hobbs, B. E. 1985. The geological significance of microfabric analysis. In: *Preferred Orientation in Deformed Metals and Rocks: An Introduction to Modern Texture Analysis* (edited by Wenk, H.-R.). Academic Press, New York, 463–484.

Jessell, M. W. 1986. Grain boundary migration and fabric development in experimentally deformed octachloropropane. *J. Struct. Geol.* **8**, 527–542.

Jessell, M. W. 1988a. Simulation of fabric development in recrystallized aggregates—I. Description of the model. *J. Struct. Geol.* **10**, 771–778.

Jessell, M. W. 1988b. Simulation of fabric development in recrystallized aggregates—II. Example model runs. *J. Struct. Geol.* **10**, 779–793.

Jessell, M. W. & Lister, G. S. 1990. A simulation of the temperature dependence of quartz fabrics. In: *Deformation Mechanism, Rheology and Tectonics* (edited by Knipe, R. J. & Rutter, E. H.). *Spec. Publs geol. Soc. Lond.* **54**, 353–362.

Kallend, J. S., Kocks, U. F., Rollett, A. D. & Wenk, R.-H. 1991. Operational texture analysis. *Mater. Sci. & Engng* **A132**, 1–11.

Karato, S.-I. 1987. Seismic anisotropy due to lattice preferred orientation of minerals: Kinematic or dynamic? In: *High-Pressure Research in Mineral Physics* (edited by Manghnani, M. H. & Syono, Y.). Terrapub, Tokyo, and American Geophysical Union, Washington, DC, 455–471.

Karato, S.-I. 1988. The role of recrystallization in the preferred orientation of olivine. *Phys. Earth & Planet. Interiors* **51**, 107–122.

Kern, H. 1977. Preferred orientation of experimentally deformed limestone marble, quartzite, and rock salt at different temperatures and states of stress. *Tectonophysics* **39**, 103–120.

Kirby, S. H. 1977. The effects of the α–β phase transformation on the creep properties of hydrolytically-weakened synthetic quartz. *Geophys. Res. Lett.* **4**, 97–100.

Kirchener, D. & Teyssier, C. 1991. Quartz *c*-axis fabric differences between porphyroclasts and recrystallized grains. *J. Struct. Geol.* **13**, 105–109.

Kirchener, D. & Teyssier, C. 1992. Quartz *c*-axis fabric differences between porphyroclasts and recrystallized grains: Reply. *J. Struct. Geol.* **14**, 631–634.

Knipe, R. J. & Law, R. D. 1987. The influence of crystallographic orientation and grain boundary migration on microstructural and textural evolution in an *S–C* mylonite. *Tectonophysics* **135**, 155–169.

Kronenberg, A. K. & Tullis, J. 1984. Flow strengths of quartz aggregates: grain size and pressure effects due to hydrolytic weakening. *J. geophys. Res.* **89**, 4281–4297.

Kunze, F. R. & Ave'Lallemant, H. G. 1981. Non-coaxial experimental deformation of olivine. *Tectonophysics* **74**, T1–T13.

Law, R. D. 1986. Relationships between strain and quartz crystallographic fabrics in the Roche Maurice quartzites of Plougastel, western Brittany. *J. Struct. Geol.* **8**, 493–515.

Linker, M. F., Kirby, S. H., Ord, A. & Christie, J. M. 1984. Effects of compression direction on the plasticity and rheology of hydrolytically weakened synthetic quartz crystals at atmospheric pressure. *J. geophys. Res.* **89**, 4241–4255.

Lister, G. S. & Hobbs, B. E. 1980. The simulation of fabric development during plastic deformation and its application to quartzite: the influence of deformation history. *J. Struct. Geol.* **2**, 355–370.

Lister, G. S., Paterson, M. S. & Hobbs, B. E. 1978. The simulation of fabric development in plastic deformation and its application to quartzite: the model. *Tectonophysics* **45**, 107–158.

Lister, G. S. & Price, G. P. 1978. Fabric development in a quartz–feldspar mylonite. *Tectonophysics* **49**, 37–78.

Mainprice, D. H. 1981. The experimental deformation of quartz polycrystals. Unpublished Ph.D. thesis, Australian National University, Canberra.

Mainprice, D., Bouchez, J.-L., Blumenfeld, P. & Tubia, J. M. 1986. Dominant *c* slip in naturally deformed quartz: Implications for dramatic plastic softening at high temperature. *Geology* **14**, 819–822.

Mainprice, D. H. Paterson, M. S. 1984. Experimental studies of the role of water in the plasticity of quartzites. *J. geophys. Res.* **89**, 4257–4270.

Mainprice, D. & Paterson, M. In press. Experimental deformation of flint. *Tectonophysics*.

Mancktelow, N. S. 1987. Atypical textures in quartz veins from the Simplon Fault Zone. *J. Struct. Geol.* **9**, 995–1005.

Masuda, T. & Fujimura, A. 1981. Microstructural development of fine-grained quartz aggregates by syntectonic recrystallization. *Tectonophysics* **72**, 105–128.

Matthies, S. 1979. On the reproducibility of the orientation distribution function of texture samples from pole figures (ghost phenomena). *Phys. Stat. Sol.* **B92**, K135–K138.

Matthies, S., Wenk, H.-R. & Vinel, G. W. 1988. Some basic concepts of texture analysis and comparison of three methods to calculate orientation distributions from pole figures. *J. Appl. Crystall.* **21**, 285–304.

Schmid, S. M. & Casey, M. 1986. Complete texture analysis of commonly observed quartz *c*-axis patterns. *Am. Geophys. Un. Geophys. Monogr.* **36**, 263–286.

Sellars, C. M. 1978. Recrystallization of metals during hot deformation. *Phil. Trans. R. Soc. Lond.* **A288**, 147–158.

Shelley, D. 1971. Hypothesis to explain the preferred orientation of quartz and calcite produced during syntectonic recrystallization. *Bull. geol. Soc. Am.* **82**, 1943–1954.

Simpson, C. & Schmid, S. 1983. An evaluation of criteria to deduce the sense of movement in sheared rocks. *Bull. geol. Soc. Am.* **94**, 1281–1288.

Toriumi, M. & Karato, S.-I. 1985. Preferred orientation development of dynamically recrystallized olivine during high temperature creep. *J. Geol.* **93**, 407–417.

Tullis, J. A. 1971. Preferred orientation in experimentally deformed quartzites. Unpublished Ph.D. thesis, University of California, Los Angeles.

Tullis, J., Christie, J. M. & Griggs, D. T. 1973. Microstructures and preferred orientations of experimentally deformed quartzites. *Bull. geol. Soc. Am.* **84**, 297–314.

Tullis, J. & Tullis, T. E. 1972. Preferred orientation produced by mechanical Dauphine' twinning. *Am. Geophys. Un. Geophys. Monogr.* **16**, 67–82.

Tullis, J. & Yund, R. A. 1982. Grain growth kinetics of quartz and calcite aggregates. *J. Geol.* **90**, 301–318.

Tullis, J. & Yund, R. A. 1985. Accommodation mechanism for dislocation creep: comparison of quartz and feldspar. *Trans. Am. Geophys. Un.* **65**, 366.

Urai, J.-L., Humphreys, F. J. & Burrows, S. E. 1980. *In situ* studies of the deformation and dynamic recrystallization of rhombohedral camphor. *J. Mater. Sci.* **15**, 1231–1240.

Wenk, H.-R., Canova, G., Molinari, A. & Kocks, U. F. 1989. Viscoplastic modeling of texture development in quartzite. *J. geophys. Res.* **94**, 17,895–17,906.

Wenk, H.-R. & Christie, J. M. 1991. Comments on the interpretation of deformation textures in rocks. *J. Struct. Geol.* **13**, 1091–1110.

Wenk, H.-R. & Kolodny, Y. 1968. Preferred orientation of quartz in a chert breccia. *Proc. nat. Acad. Sci.* **59**, 1061–1066.

Wilson, C. J. L. 1986. Deformation induced recrystallization of ice: The application of *in situ* experiments. *Am. Geophys. Un. Geophys. Monogr.* **36**, 213–232.

White, S. H. 1976. The effects of strain on microstructures, fabrics, and deformation mechanisms in quartzites. *Phil. Trans. R. Soc. Lond.* **A283**, 69–86.